The aqueous chemistry of element 104 rutherfordium : cation exchange behavior of fluoro complexes

THESIS

The Aqueous Chemistry of Element 104 Rutherfordium

- Cation exchange behavior of fluoro complexes -

Yasuo Ishii

Graduate School

of

Science and Engineering

Shizuoka University

May, 2008

Abstract

Fluoride complexation of the transactinide element, rutherfordium (Rf), belonging to the group-4 in the 7th row of the periodic table was investigated through cation-exchange chromatography based on an atom-at-a-time scale. Cation-exchange behavior of Rf was systematically studied in hydrofluoric and nitric acid (HF/HNO_3) mixed solutions as a function of the concentration of the fluoride ion [F^-] and the hydrogen ion [H^+] concentrations together with its lighter homologues zirconium (Zr) and hafnium (Hf), and the tetravalent pseudo-homologue thorium (Th).

The nuclide ^{261}Rf with a half-life ($T_{1/2}$) of 78 s was used for the chemical study of Rf. Rutherfordium-261 was produced in the ^{18}O-induced nuclear reaction with a ^{248}Cm target with a production rate of about 2 atoms per min at the JAEA (Japan Atomic Energy Agency) tandem accelerator. Reaction products recoiling from the target foil were stopped in helium gas loaded with potassium chloride (KCl) aerosols. Then the products adsorbed on the surface of the aerosols were continuously transported through a capillary to the chemistry laboratory within a few seconds. Because of the short half-life and the low production rate of ^{261}Rf, each Rf atom produced decays before a new atom is synthesized. Thus, chemical experiments with ^{261}Rf were conducted on an atom-at-a-time scale.

Cation-exchange experiments on Rf were carried out using an automated rapid ion-exchange separation apparatus that enables us to perform cyclic column chromatographic separations. The transported products were collected on a deposition site of the apparatus for 130 s. Then, the products were dissolved with 250 μL of the mixed HF/HNO_3 solutions and were subsequently fed onto micro columns (1.6 mm i.d. × 7.0 mm and 1.0 mm i.d. × 3.5 mm) filled with a cation-exchange resin. The effluent was collected on a tantalum (Ta) disk as fraction 1, while the remaining products in the column were stripped with 250 μL of 0.1 M

HF/0.1 M HNO_3 and the effluent was collected on another Ta disk as fraction 2. Both samples were evaporated to dryness using hot He or N_2 gas and a halogen heat lamp. The pair of disks was automatically transferred to an α-spectrometry station to identify the nuclide through its α-decay energy. From the radioactivities of ^{261}Rf observed in fractions 1 and 2, the adsorption probability on the cation-exchange resin was determined. Cation-exchange behavior of the homologues on the same resin was separately studied by a batch-wise method using radiotracers and by the same on-line column chromatographic methods as those with ^{261}Rf.

Distribution coefficients (K_d) of Rf evaluated from the adsorption probability and those of the homologues were measured as a function of $[F^-]$ at the constant nitric acid concentration $[HNO_3]$ = 0.10 M. It was found that the K_d values of Zr, Hf and Th decrease with increasing $[F^-]$ due to the consecutive formation of fluoro complexes of those elements. The K_d values of Rf also decreased with an increase of $[F^-]$ being between those of Zr/Hf and Th. The result suggested that the fluoride complexation of Rf successively proceeds in the same way as for the homologues.

The K_d values of Rf and the homologues were measured as a function of $[H^+]$ at constant $[F^-]$. The result indicated that the logK_d values of those elements linearly decrease with an increase of log$[H^+]$ with the slopes of -2.5. This means that these elements are likely to be present in the same forms with the mixture of $[MF]^{3+}$ and $[MF_2]^{2+}$ (M = Rf, Zr, Hf and Th) in the studied solutions. From these results, it is ascertained that the strength of the coordination of the fluoride ions to Rf to form the complexes $[MF]^{3+}$ and/or $[MF_2]^{2+}$ is significantly weaker than that to Zr and Hf, but it is stronger than that of Th.

Since the fluoride ion is a hard base, the metal fluoro complexes serve as good models for the ionic and electrostatic interaction; the fluoride complexation strongly correlates with the electronic densities of the metal cations that originate from their size and charges. The observed

sequence of the fluoride complexation, Zr ~ Hf > Rf > Th, suggests a strong correlation between the complexing strength and the size of the tetravalent metal cations. The ionic radii of Zr^{4+}, Hf^{4+}, Rf^{4+} and Th^{4+} are reported as 72 pm, 71 pm, 76 pm and 94 pm, respectively, where the radii of Zr^{4+}, Hf^{4+} and Th^{4+} are taken from the structural data, while that of Rf is the theoretically predicted value from relativistic atomic orbital calculations. The present result clearly indicates that the size of Rf^{4+} would be in between those of Zr^{4+}/Hf^{4+} and Th^{4+}.

The Aqueous Chemistry of Element 104 Rutherfordium

- Cation exchange behavior of fluoro complexes -

Chapter 1

Introduction

1-1. Background

Chemistry is the science about the materials, concerned with structure, properties and reactions. All the materials consists of atoms and these characters are related with states and interactions of each atom. It is said that the genesis of chemistry is alchemy. Concepts of the transmutation of lead into gold was succeeded to the nuclear transmutation and many new elements have been artificially produced by nuclear scientists through the past time. Presently, we know more than 20 artificial transuranium elements. The elements with atomic numbers $Z \geq 104$ are called transactinide elements [1-5].

The currently known transactinide elements, elements 104 through 112, are placed in the periodic table under their respective lighter homologues in the 5d electron series, hafnium (Hf) to mercury (Hg). Elements from 113 to 118 with the exception of 117 synthesized would be in the successive 7p electron series, although the discoveries of elements with $Z \geq 112$ are still waiting to be confirmed (see Fig. 1-1).

Chemical characterization of the newly-synthesized transactinide elements is an extremely fascinating and challenging subject in modern nuclear and inorganic chemistry [1-5]. Most important and interesting question is to clarify chemical properties of these elements at the uppermost end of the periodic table and to elucidate the influence of relativistic effects in chemical properties of the heaviest elements [6, 7].

1-2. Production of heavy elements

The transuranium elements with $Z \geq 93$ are artificially produced in nuclear reactions [8]. Up to fermium ($Z = 100$), neutron capture in high-flux reactors and successive β^- decay make it possible to climb up the periodic table element by element. The elements with atomic numbers $Z \geq 101$, called "the heaviest elements", cannot be produced in the neutron capture

reactions. These elements must be produced only in heavy-ion-induced nuclear reactions, i.e., the bombardment of heavy element targets with heavy ions from an accelerator [8]. From a limitation of an available target amount due to energy loss of heavy ions, the production rate of the heaviest elements is very small relative to that of the neutron capture reactions. In addition, because the production cross sections become lower with an increase of Z of the reaction products, the production rates of these elements are extremely low. Moreover, nuclear half-lives of the transactinide elements are very short in the order of a minute to seconds. Thus, each atom produced decays before a new atom is synthesized. This means that any chemical experiment to be performed must be done on an atom-at-a-time scale.

1-3. Atom-at-a-time chemistry

In a chemical process, chemical equilibrium is one of the most important state in which these are no changes in chemical activities or concentrations of each phase (organic - aqueous phase, reactants - products, etc.) over time. The atom-at-a-time chemistry has to be carried out on phenomena that give the same results for single atoms and for macro amounts of atoms; the question arises as to whether a meaningful chemistry with single atoms is possible.

For singe atoms, in a two-phase distribution reaction, the atom cannot exist in both phases taking part in the chemical equilibrium at the same time. Thus, for single atom chemistry, a specific thermodynamic function has to be introduced.

Guillaumont *et al.* [9, 10] introduced the concept of the "single particle free enthalpy" as a new thermodynamic function for one atom involved in a system, which is obtained by comparing the free enthalpy derived from the partition function between the molecules with the Stirling's approximation and one molecule without the approximation. According to this law, an equilibrium constant (distribution coefficient) of the atom between two phases is correctly

defined in terms of the probabilities of finding the atom in one phase or the other. If a static partition method is used, this coefficient must be measured in repetitive experiments. Since dynamical partition methods can be considered as repetitive static partitions, the displacement of the atom along the chromatographic column gives a statistical result. The concept of single atom chemistry is depicted in Fig. 1-2.

1-4. Previous chemical studies of rutherfordium

Element 104, rutherfordium is the first appearing transactinide and 6d transition element placed in the 7th row of the periodic table [11] as shown in Fig. 1-1.

The chemical experiments with the transactinide elements have been conducted together with the homologues under identical conditions to compare the properties with those of the homologues. The pioneering solution chemistry of Rf produced by irradiation of ^{248}Cm with ^{18}O ions by Silva *et al.* [12] on the cation-exchange separation clearly demonstrated that the adsorption behavior of Rf is entirely different from that of the trivalent actinide elements but similar to that of Zr and Hf in group-4. Hulet *et al.* [13] also revealed that the chloride complexation of Rf is much stronger than that of the trivalent actinide elements and is similar to that of Hf. Another early work on the chemical study of Rf focused on gas thermochromatographic studies by Zvara *et al.* [14] showed that volatility of Rf tetrachloride was similar to those of Zr and Hf, indicating that they have similar chemical properties and belong to the same element group.

Recently, more detailed studies of Rf were performed. As the fluoride ion is a very strong coordinating agent for the group-4 elements, several studies of Rf were conducted in hydrofluoric acid (HF) and in mixed solutions of HF with other acids, such as nitric acid (HNO_3) and hydrochloric acid (HCl) solutions. Kacher *et al.* [15] first reported the fluoride

complexation of Rf. The extraction sequence of the group-4 elements from 0.5 M HF into TIOA (triisooctylamine) is in the following order: Ti > Zr = Hf > Rf. Subsequent studies of the fluoride complexation of Rf using ion-exchange techniques were carried out by Szeglowski *et al.* [16], Pfrepper *et al.* [17], Strub *et al.* [18], Kronenberg *et al.* [19] and Schumann *et al.* [20].

The first interesting results on cation- and anion-exchange behavior of Rf in HF/0.1 M HNO_3 solution was reported by Strub *et al.* [18]; the cation exchange behavior of Rf is similar to that of Th, not those of Zr and Hf, while the anion-exchange behavior of Rf is different from those of Zr and Hf, where distribution coefficient (K_d) values in both batch and column experiments were defined as a ratio of specific radioactivities between the aqueous and resin phases. Later, the K_d values were re-evaluated [19] with the simulation of the elution process based on the Glueckauf equation [21]. The re-evaluated cation-exchange behavior of Rf was intermediate between those of Zr/Hf and Th, while the re-evaluated anion-exchange behavior of Rf seemed to be different from the homologues Zr and Hf.

However, the above mentioned experiments have the following problems: 1) insufficient counting statistics, 2) lack of reliability due to the re-evaluation of the K_d values and 3) no information on chemical species and chemical equilibria of Rf. Then, Haba *et al.* [22] and Toyoshima *et al.* [23, 24] studied fluoride complexation of Rf through anion-exchange chromatography together with the lighter homologues Zr and Hf in HF and in HF/HNO_3 mixed solutions with enough statics. These results revealed that the ion-exchange behavior of Rf is remarkably different from that of Zr and Hf, and that the fluoride complexation of Rf is much weaker than that of the homologues. Recently, Toyoshima *et al.* [24] proved the formation of the hexafluoro complex of Rf, $[RfF_6^{2-}]$, like $[ZrF_6^{2-}]$ and $[HfF_6^{2-}]$ which made it possible to more detailed discussion of interaction between Rf and the fluoride ion F^-.

1-5. Aim of this work

The present study is to deepen further the understanding of the fluoride complex formation of Rf and to obtain information about the size of the ionic radius of Rf^{4+}.by using a cation-exchange chromatographic method. Consecutive fluoride complex formation of Rf and the strength of the fluoride complexation of Rf compared with that of Zr and Hf and thorium (Th) were investigated in the HF/HNO_3 mixed solution.

Distribution coefficients (K_d value) of Zr, Hf and Th on cation-exchange resin were measured under static conditions, i.e., by batch experiments using the long-lived radiotracer ^{88}Zr, ^{175}Hf and ^{234}Th. In the cation-exchange chromatography, Th, a member of the actinide series, can be used as a comparative element to that of the group-4 elements. To avoid any reactions of metallic ions with each other such as polymerization, the carrier-free radioactive tracers were prepared. The cation-exchange behavior of ^{261}Rf was investigated together with the homologue isotopes ^{85}Zr and ^{169}Hf under dynamic conditions, i.e., by chromatographic experiments using Automated Ion exchange separation apparatus coupled with the Detection system for Alpha spectroscopy (AIDA). Distribution coefficients for these elements are systematically measured as a function of the concentration of the fluoride ion $[F^-]$ and of the hydrogen ion $[H^+]$. To examine the coordination of the nitrate ion (NO_3^-), the variation of distribution coefficients of Zr, Hf and Th was also obtained using the less coordinating ion, perchlorate ion (ClO_4^-) as a function of the concentration of the hydrogen ion $[H^+]$.

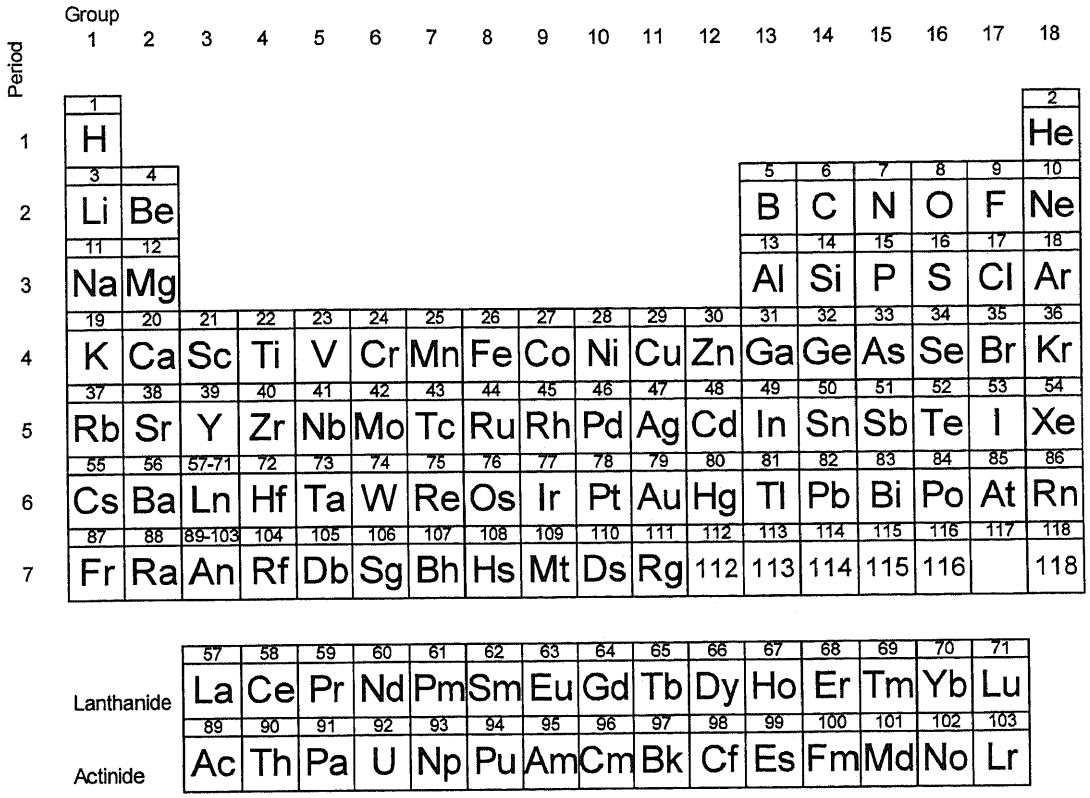

Fig. 1-1. Periodic table of the elements.

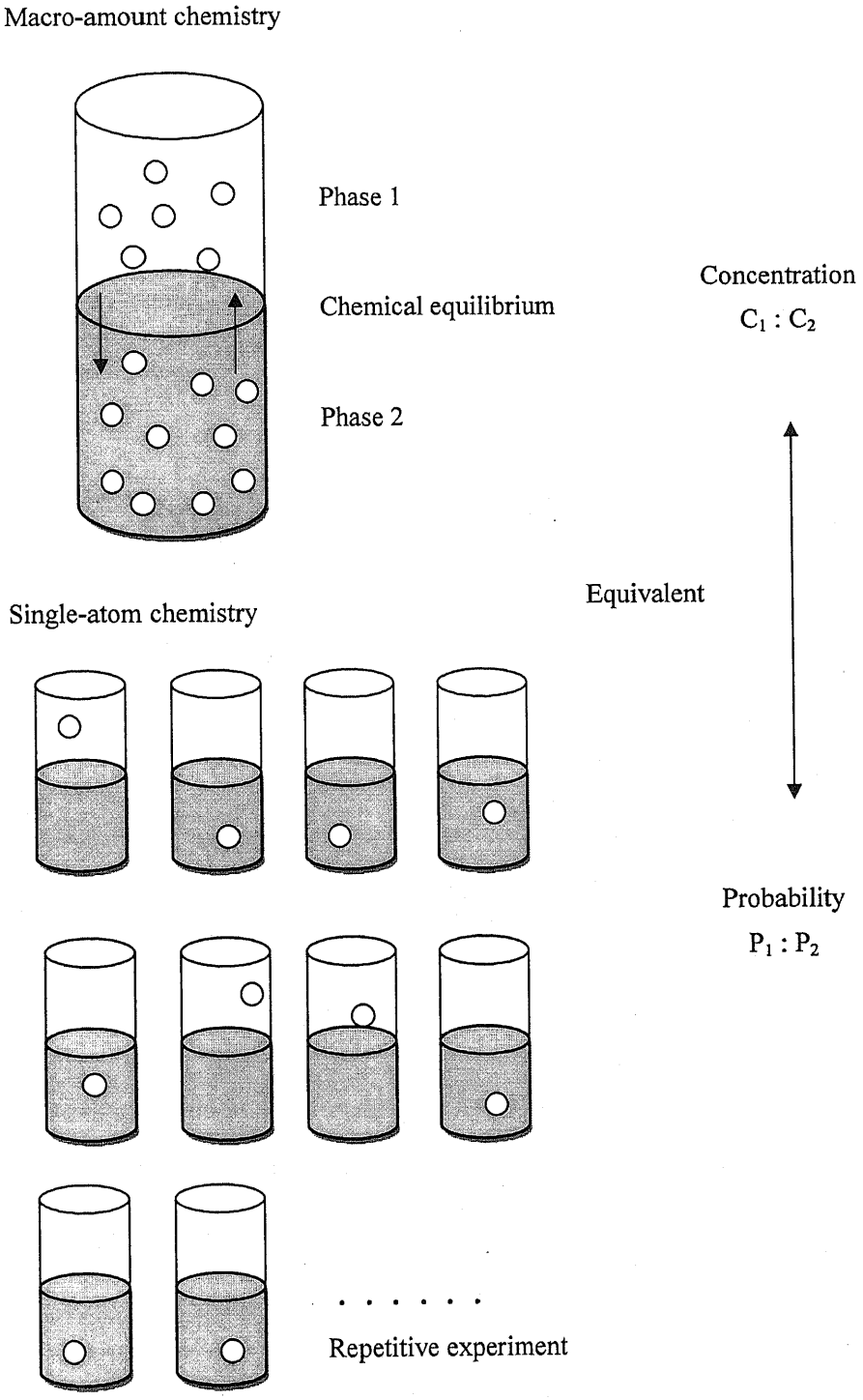

Fig. 1-2. Concept of atom-at-a-time (single atom) chemistry.

Chapter 2

Experimental procedures and Apparatus

2-1. Experimental procedures of batch experiments

2-1-1. Production of radiotracers ^{88}Zr and ^{175}Hf

The carrier-free radiotracers ^{88}Zr ($T_{1/2}$ = 83.4 d) and ^{175}Hf ($T_{1/2}$ = 70.0 d) were produced in the reactions ^{89}Y(p, $2n$) and ^{175}Lu(p, n), respectively at the JAEA tandem accelerator. A stack of ^{89}Y (99.9% purity, 7 mm × 7 mm, 0.25 mm thick) and ^{175}Lu (99.9% purity, 6 mm × 6 mm, 0.127 mm thick) metallic foils covered with an Al foil was irradiated with the 14.2 - 27.8 MeV and 6.1 - 12.5 MeV proton beams, respectively in a vacuum chamber.

The irradiated Y and Lu targets were dissolved with concentrated HCl (conc. HCl) and were evaporated to dryness twice. Then, the residues were dissolved with conc. HCl and were fed onto an anion-exchange column (DIAION SA#100, 100-200 mesh, Cl^- form, 4 mm i. d. × 40 mm). After washing the column with conc. HCl, the fractions of ^{88}Zr and ^{175}Hf were eluted with 4 M HCl. The schematic diagrams of the preparation procedures for ^{88}Zr and ^{175}Hf are shown in Figs. 2-1 and 2-2, respectively. The prepared radiotracers were stored in polypropylene vessels in 0.10 or 2.0 M HNO_3, or 0.10 or 2.0 M $HClO_4$ solutions.

2-1-2. Preparation of a radiotracer ^{234}Th

Thorium-234 is a daughter nuclide of naturally occurring radioactive ^{238}U. Commercially available $UO_2(NO_3)_2 \cdot 6H_2O$ was dissolved with 9.0 M HCl and was fed onto the anion-exchange resin (DIAION SA#100, 100-200 mesh, Cl^- form, 28 mm i. d. × 300 mm). The effluent was evaporated to dryness and dissolved with 9.0 M HNO_3 and was fed onto another anion-exchange column (Dowex 1 × 8, 200-400 mesh, NO_3^- form, 4 mm i. d. × 40 mm). After washing the column with 9.0 M HNO_3, ^{234}Th was eluted with 0.10 M HCl. The schematic diagram of the preparation procedures of ^{234}Th is shown in Fig. 2-3. After evaporation of the solution containing the ^{234}Th tracer

to dryness, the residues was dissolved in 0.10 or 2.0 M HNO_3, or 0.10 or 2.0 M $HClO_4$ solutions.

2-1-3. Chemicals

The cation-exchange resin used in the batch experiment was MCI GEL CK08Y, supplied by Mitsubishi Chemical Corporation, a strongly acidic quaternary-amine polymer with a particle size of 20 μm. The resin was stirred alternatively in 4.0 M HCl and 4.0 M NaOH solutions 5 times and converted to the hydrogen (H^+) form by washing in 4.0 M HCl solution. Then it was washed with distilled water several times until neutral solution was obtained, and was dried up to a constant weight at 110 ℃ in a vacuum oven. The dried resin was kept in a desiccator.

All the chemicals were of the reagent grade without any purification. The concentration of HNO_3 and $HClO_4$ solutions was determined by titration with Na_2CO_3 solution, while the concentration of HF was determined by titration with NaOH solution.

2-1-4. Batch experiments with the radiotracers

A portion of 10 - 200 mg of CK08Y and 3.0 mL of the HF/HNO_3 or HF/$HClO_4$ solution containing 50 μL of the tracer solution were added into a polypropylene tube and were shaken for 3 h at 20 ℃. After centrifugation, 1.0 mL of the aqueous phase was precisely pipetted into a polyethylene tube and subjected to γ-ray spectrometry using a Ge detector. As a standard sample, 50 μL of the tracer solution was diluted to 3.0 mL with the same HF/HNO_3 or HF/$HClO_4$ solution in another polyethylene tube. Because it is difficult to measure radioactivities in the resin phase with the same counting efficiency as an aqueous phase, the radioactivity in the resin phase (A_{Resin}) was calculated using $A_{Resin} = A_{Standard} - A_{Solution}$, where $A_{Solution}$ and $A_{Standard}$ are the radioactivity in the aqueous phase and the initial radioactivity obtained from a standard sample, respectively. The number of ^{88}Zr, ^{175}Hf and ^{234}Th atoms used for each batch experiment was about 10^{10}.

2-2. On-line experimental procedures and apparatus

2-2-1. Production of short-lived nuclides ^{85}Zr and ^{169}Hf

To investigate the behavior of Zr and Hf in cation-exchange chromatography, the short-lived nuclides ^{85}Zr ($T_{1/2}$ = 7.86 min) and ^{169}Hf ($T_{1/2}$ = 3.24 min) produced at the JAEA tandem accelerator were used in the on-line experiments. The nuclides ^{85}Zr and ^{169}Hf were simultaneously produced in the ^{nat}Ge(^{18}O, *xn*) and ^{nat}Gd(^{18}O, *xn*) reactions, respectively (nat = natural isotopic abundance) using the Gd/Ge mixed target at the ^{18}O beam energy of 89 - 91 MeV. The beam current was 200 - 300 particle nA.

The mixed target was prepared as schematically shown in Fig. 2-4. Gadolinium was electrodeposited [25] onto a 2.65 mg cm^{-2} Be foil in thickness with the area of 12.5 mm × 12.5 mm. Weighted $^{nat}Gd_2O_3$ powder was dissolved in 230 μL of 0.10 M HNO_3 solution, resulting in 339.5 μg $^{nat}Gd_2O_3$ per μL. The Be foil was placed at the bottom of the glass-cell of 5 mm diameter which was held in place by clips on an aluminum (Al) plate served as a cathode. About 3 mL of 2-propaol solution and 5 μL aliquots of the ^{nat}Gd solution were added into the cell, then a platinum (Pt) rod of 1 mm diameter served as an anode was inserted into the cell. The potentials of 700-1000 V were applied between the positive and negative electrodes for 5 min. The set up of electrodeposition is schematically shown in Fig. 2-5. After the electrodeposition, the ^{nat}Gd target was placed in an electric furnace at 500 ℃ for 15 min to convert the nitrate into the oxide.

On the resulting ^{nat}Gd target, ^{nat}Ge was deposited by vacuum evaporation [25]. The ^{nat}Gd target was sandwiched between Al holders with a hole of 5 mm diameter at a distance of 25 mm from a Mo boat on which small pieces of the metallic Ge of 33.86 mg was placed. At 3 × 10^{-5} Torr, ^{nat}Ge was evaporated with the heat generator by supplying a current of 45 A to the Mo boat and was deposited on the surface of the Gd target. Figure 2-6 shows a schematic view of the vacuum

evaporation system. As a result, the Gd/Ge mixed target was made of 370 μg cm^{-2} ^{nat}Gd and 660 μg cm^{-2} ^{nat}Ge in thickness.

2-2-2. Production of ^{261}Rf

The nuclide ^{261}Rf ($T_{1/2}$ = 78 s) produced in the ^{248}Cm(^{18}O, 5*n*) reaction was used for the chemical studies of Rf. A beam intensity of ^{18}O delivered from the JAEA tandem accelerator was 250-300 particle nA and the incident beam energy was 94 MeV on the Cm target. At this incident energy, the excitation function for the ^{248}Cm (^{18}O, 5*n*) reaction exhibits the maximum cross section of 13 nb [26]. This results in an expected production rate of about 2 atoms per minute under the present condition. The Cm target also contained the enriched ^{152}Gd to simultaneously produce short-lived Hf isotopes that are used to determine the adsorption behavior of Hf and its chemical yield.

The nuclide of ^{248}Cm (the isotopic composition: 1.12% ^{244}Cm, 1.31% ^{246}Cm and 97.32% ^{248}Cm) and ^{152}Gd (the isotopic composition: 39.3% ^{152}Gd, 5.9% ^{154}Gd, 16.7% ^{155}Gd, 13.8% ^{155}Gd, 7.7% ^{157}Gd, 10.0% ^{158}Gd and 6.6% ^{160}Gd) used for the target materials were purified by an ion-exchange method. These target materials, Cm_2O_3 and Gd_2O_3, were dissolved in 0.2 mL of 50% vol. 3.0 M HCl - 50% vol. methanol (CH_3OH) mixed solution. The solution was fed onto a cation exchange column (DIAION SK#1). After co-washing the beaker with 0.2 mL of 50% vol. 3.0 M HCl - 50% vol. CH_3OH mixed solution 4 times, 1 mL of the mixed solution was fed onto the column 3 times. Contaminants, such as Pb etc., were eluted in this fraction. Then, 0.5 mL of 6.0 M HCl solution was fed onto the column 4 times. This effluent was evaporated to dryness. Then, the residue of the ^{248}Cm and Gd fraction was dissolved with 0.2 mL 1.0 M HCl and was fed onto an anion-exchange column (Dowex 1 × 8) to further remove impurities, such as Pb. The beaker containing the residue was co-washed with 0.2 mL of

1.0 M HCl 2 times. The effluent was collected in a quartz tube vessel with a few mL of capacity. After evaporation to dryness, the residue was dissolved with 0.2 mL of conc. HNO_3 in order to convert the coordinated Cl^- ion into the NO_3^- ion of Cm and Gd. The solution was evaporated to dryness again. Then, it was dissolved with 30 μL of 0.10 M HNO_3 solution that was used for the $^{248}Cm/^{152}Ge$ stock solution for electrodeposition.

The Cm/Gd mixed target was prepared by electrodeposition [25] onto a Be foil. The Be foil of 1.805 mg cm^{-2} in thickness with the area of 12.5 mm × 12.5 mm was placed at the bottom of an electrodeposition quartz-cell with 5 mm diameter and was held in place by clips on an Al plate served as a cathode. About 3 mL of 2-propaol solution and 10 μL of the $^{248}Cm/^{152}Gd$ in 0.10 M HNO_3 solution were added into the cell. A rhodium (Rh) rod with 1 mm diameter as an anode was inserted into the cell as shown in Fig. 2-5. Six hundred volts were applied between the electrodes for 20 min. The above plating procedures were repeated several times to get a desired thickness. The thickness of the resulting Cm/Gd target was 540 μg cm^{-2} for the ^{248}Cm isotope and 32 μg cm^{-2} for the ^{152}Gd isotope. The preparation procedure is basically the same as that shown in Fig. 2-4.

2-2-3. Gas-jet transport system

Reaction products recoiling out of the target were transported rapidly by a He/KCl gas-jet system to a chemistry laboratory [27].

Figure 2-8 shows a schematic diagram of the He/KCl gas-jet system. Potassium chloride (KCl) aerosols are produced by sublimation from the surface of the KCl powder situated on a quartz boat installed in a stainless tube at 640 ℃ in an electric furnace. Helium gas flows through the stainless tube and sweeps out the KCl aerosols which undergo a large temperature drop upon leaving the furnace. This sudden drop of the temperature produces a

super-saturated KCl vapor which condenses into relatively large aerosol particles. The aerosols were fed into the target chamber through a Teflon capillary. Figure 2-9 shows a sectional view of the target chamber. The beam passed through 2.0 mg cm^{-2} HAVER vacuum window and 0.10 mg cm^{-2} of He cooling gas before entering the target chamber. The reaction products were stopped in He gas (~ 90 kPa), attached to the KCl aerosols in the target chamber, and were continuously transported through a Teflon capillary (2.0 mm i.d. and 25 m long) to a rapid chemical separation apparatus by the He gas flow at a flow rate of 2.0 L min^{-1} within a few seconds. The amount of the collected KCl aerosols in each experimental run is estimated to bo less than several tens μg, thus it does not affect the chemical behavior of the transported products.

2-2-4. Automated Ion-exchange separation apparatus coupled with the Detection system for Alpha spectroscopy (AIDA)

On-line cation-exchange chromatography was performed with AIDA (Automated Ion-exchange separation apparatus coupled with the Detection system for Alpha spectroscopy) [28] that consists of a modified ARCA (Automated Rapid Chemistry Apparatus) which is a miniaturized computer controlled high performance liquid chromatography (HPLC) system [29] and an automated on-line α-particle detection system. Figure 2-10 represents a schematic of AIDA.

The modified ARCA consists of (i) body blocks with tiny holes to pass solutions, (ii) a central slider for the collection of the transported products by the He/KCl gas-jet, (iii) symmetrically placed two column holders each of which is equipped with 20 microcolumns for chromatographic separation, and (iv) the peripheral parts such as pneumatically driven four-ways slider valves, chemically inert HPLC pumps, Teflon tubes and so on. The use of the

two-microcolumn system through a parallel running allows us to avoid a waste of time for chemical separation. The minimized body reduces the dead volume of the system which makes rapid preparation of the α-counting samples. The operation of the apparatus is controlled by a computer. In the modified ARCA as shown in Fig. 2-11, two different paths to supply solutions are available; the first eluent goes through the collection site to the microcolumn, while the other one is directed to the column after one-step forward movement of the column holder to avoid cross-contamination at the collection site. AIDA enable us to perform cyclic column chromatographic separations of short-lived nuclides in aqueous solutions and automated detection of α-particles within a typical cycle of 1-2 min. Fig. 2-12 shows the schematic flow a present liquid chromatographic experiment with Rf.

2-2-5. Chemicals

The cation-exchange resin used in the on-line experiments was MCI GEL CK08Y prepared by the same method in the batch experiment.

All the chemicals were of the reagent grade without any purification. The concentration of HNO_3 solution was determined by titration with Na_2CO_3 solution, while the concentration of HF was determined by titration with NaOH solution.

2-2-6. Cation-exchange chromatography of ^{85}Zr and ^{169}Hf

In order to investigate the behavior of the short-lived ^{85}Zr and ^{169}Hf in cation-exchange chromatography, elution curves of these nuclides were measured with AIDA in HF/0.10 M HNO_3. For the measurement of a wide range of K_d values, two kinds of the microcolumns, 1.6 mm i. d. × 7.0 mm and 1.0 mm i. d. × 3.5 mm, were used. These were filled with the cation exchange resin (MCI GEL CK08Y). The reaction products transported by the He/KCl gas-jet

method from the Ge/Gd target were collected on the deposition site of AIDA for 60-180 s. The collected products were dissolved in the 10^{-2} - 10^{-4} M HF/0.10 M HNO_3 solutions and were subsequently fed onto the cation-exchange column at a flow rate of 0.70 mL min^{-1}. The effluent was fractionated in seven aliquots which were separately collected in seven polyethylene tubes. The remaining products in the column were eluted with 1.00×10^{-1} M HF/0.10 M HNO_3 at a flow rate of 1.0 mL min^{-1} and were collected in another polyethylene tube. The 416 keV and 370 keV γ-rays of ^{85}Zr and ^{169}Hf, respectively, in each tube were measured with a Ge detector.

The number of ^{85}Zr and ^{169}Hf atoms used for each on-line experiment was about 10^4 - 10^6.

2-2-7. Cation-exchange chromatography of ^{261}Rf and ^{169}Hf

Because it is difficult to directly measure the distribution coefficient (K_d) values of ^{261}Rf from its elution curves, adsorption probabilities on the resin were measured in the present chromatographic experiment with Rf.

Reaction products recoiling out of the target were transported by the He/KCl gas-jet system to the chemistry laboratory. The transported products were deposited on the collection site of AIDA for 130 s. Then, the products were dissolved and fed onto the column with 250 μL of HF/HNO_3 solutions at a flow rate of 0.7 mL min^{-1}. The effluent (fraction 1) was collected on a Ta disk and evaporated to dryness using hot He or N_2 gas and a halogen heat lamp. The remaining products in the column were eluted with 250 μL of 1.00×10^{-1} M HF/0.10 M HNO_3 at a flow rate of 1.0 mL min^{-1}. The effluent (fraction 2) was collected on another Ta disk and evaporated to dryness in the same manner. These experiments were performed at room temperature (25 ± 1 ℃).

The pair of disks was automatically transferred to an α-spectrometry station equipped

with 600 mm^2 PIPS (Passivated Implanted Planar Silicon) detectors. From observed radioactivities, we evaluated the adsorption probability and the K_d value of Rf on the cation-exchange resin. The percent adsorption (%ads) value on the resin is defined as %ads = $100A_2/(A_1 + A_2)$ with the radioactivities of A_1 and A_2 (Bq) in fractions 1 and 2, respectively.

After the α-particle measurement, every third pair of disks was sampled and the 493 keV γ-ray of ^{169}Hf was measured with Ge detectors to monitor the chemical yield and adsorption behavior of Hf. The chemical yield of Hf was approximately 60% and no adsorption of Hf was observed on the cation exchange resin at the present conditions. This procedure is schematically shown in Fig, 2-13. Typical time sequence of the cation-exchange chromatographic method of the Rf experiment is shown in Fig. 2-14. Each separation was accomplished within 25 s and the α-particle measurement was started within 80 s for the 1st fraction after the collection of the products at the AIDA collection site.

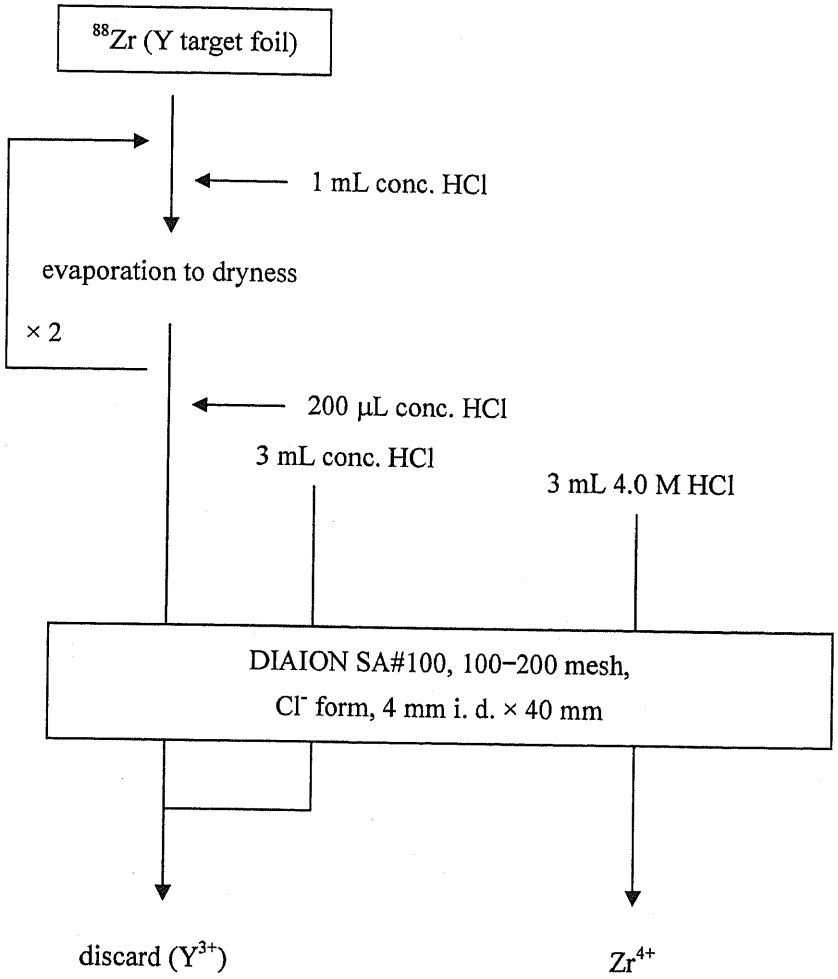

Fig. 2-1. Separation scheme for the preparation of the carrier free ^{88}Zr isotope from the irradiated Y target foil.

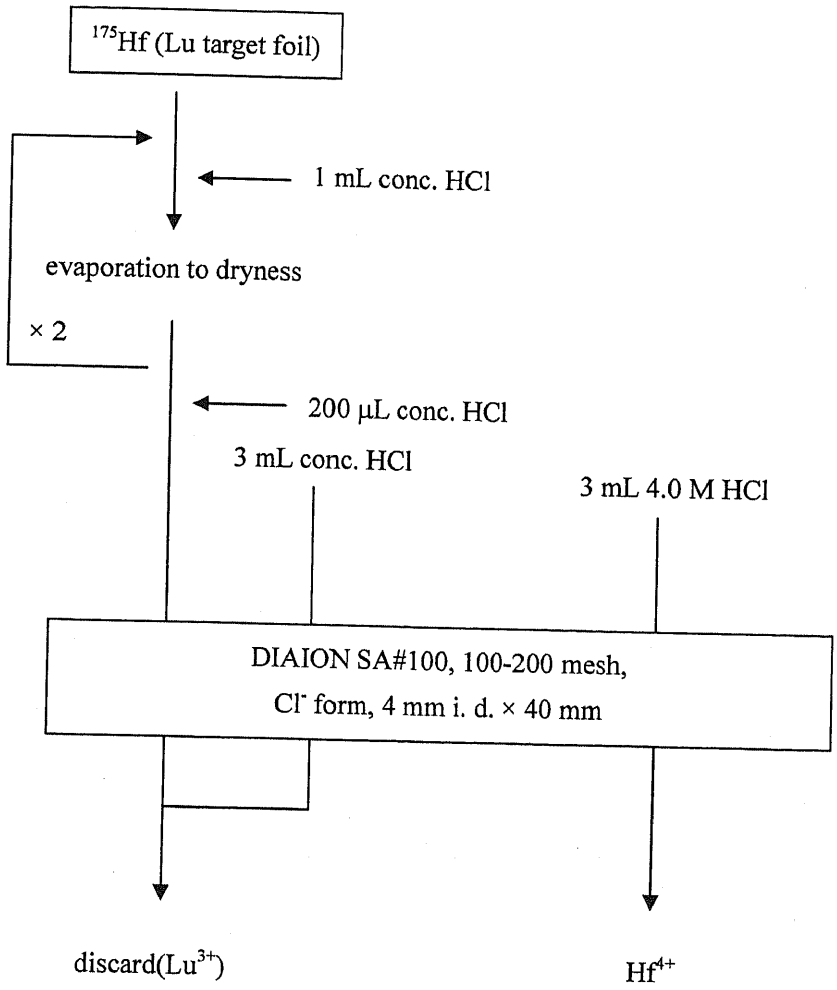

Fig. 2-2. Separation scheme for the preparation of the carrier free ^{175}Hf isotope from the irradiated Lu target foil.

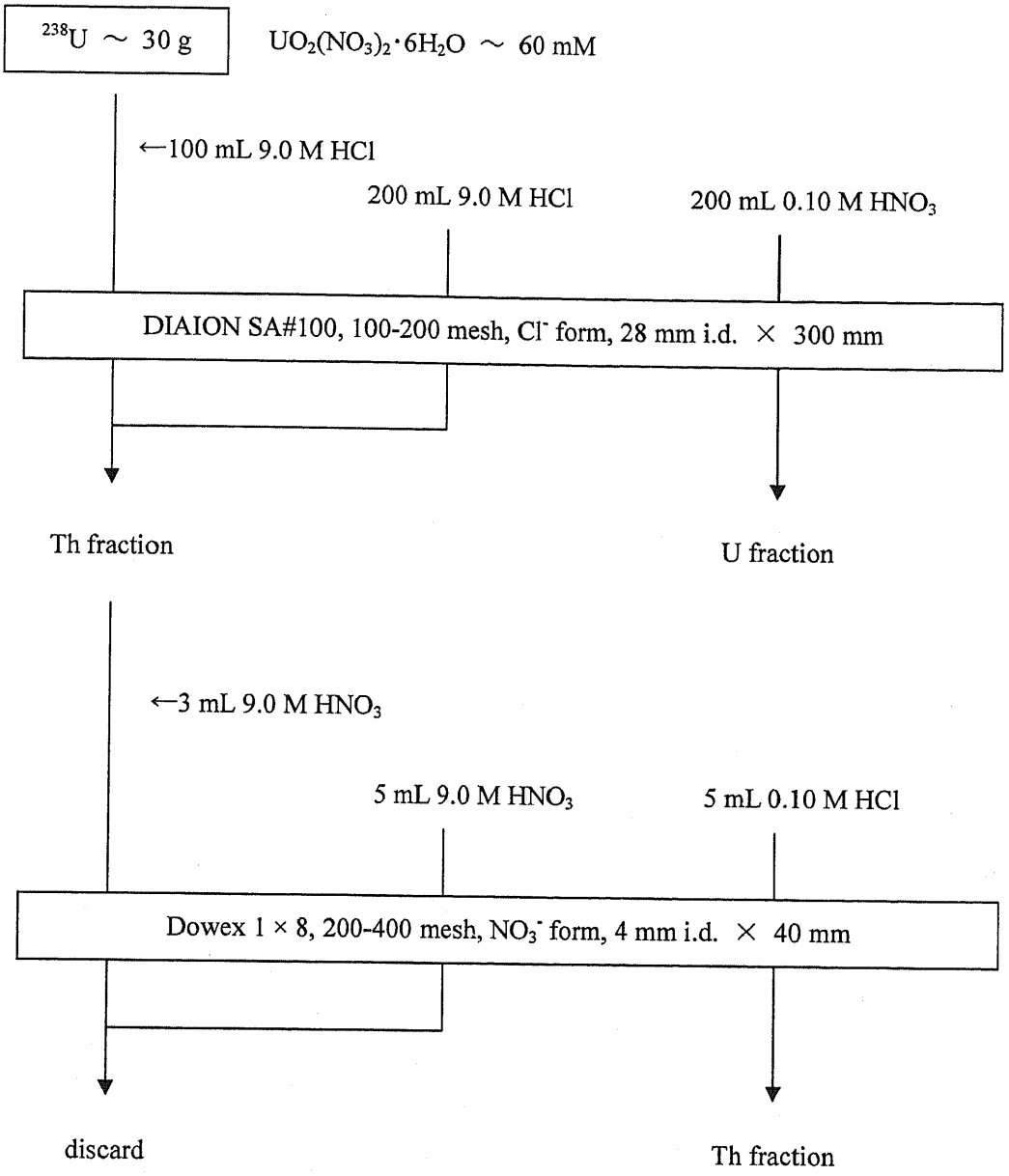

Fig. 2-3. Separation scheme for the preparation of ^{234}Th from the naturally occurring uranium, $UO_2(NO_3) \cdot 6H_2O$.

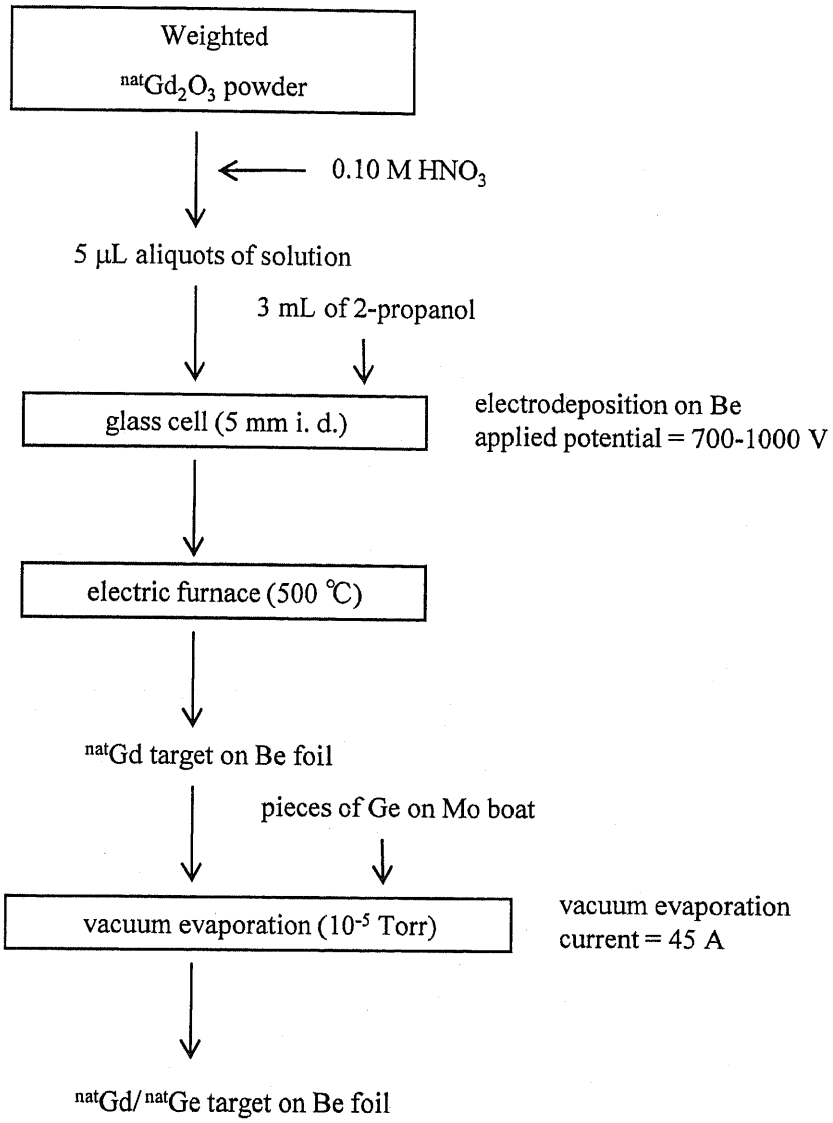

Fig. 2-4. Schematic diagram of the preparation procedures of the Gd/Ge mixed target.

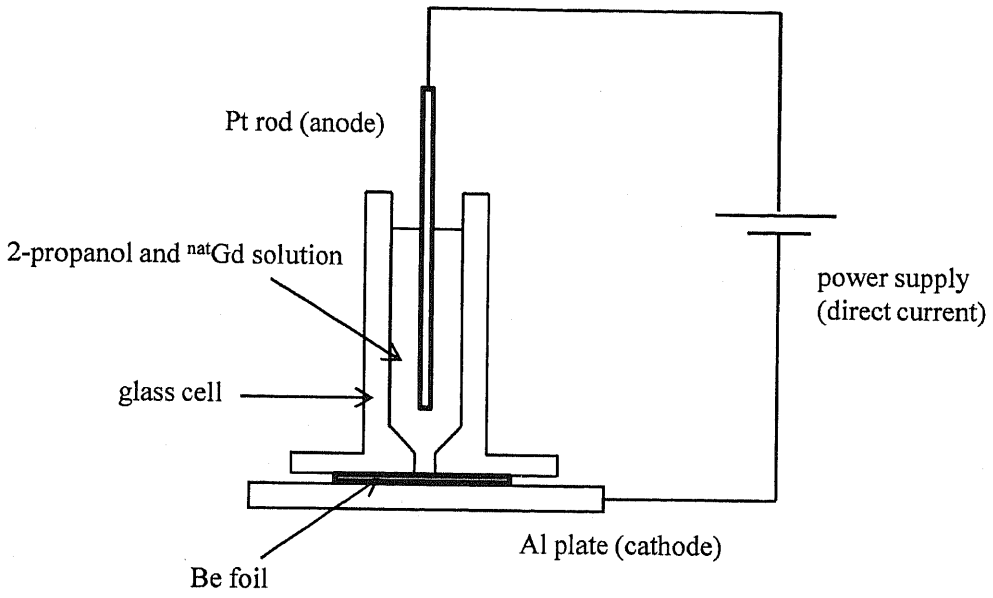

Fig. 2-5. Cross sectional view of the set up for electrodeposition of Gd.

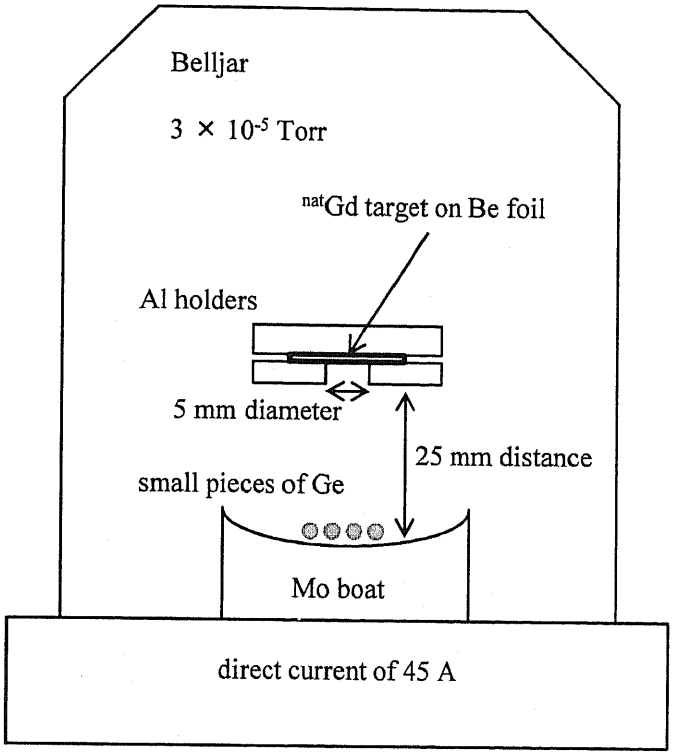

Fig. 2-6. Schematic view of the vacuum evaporation system.

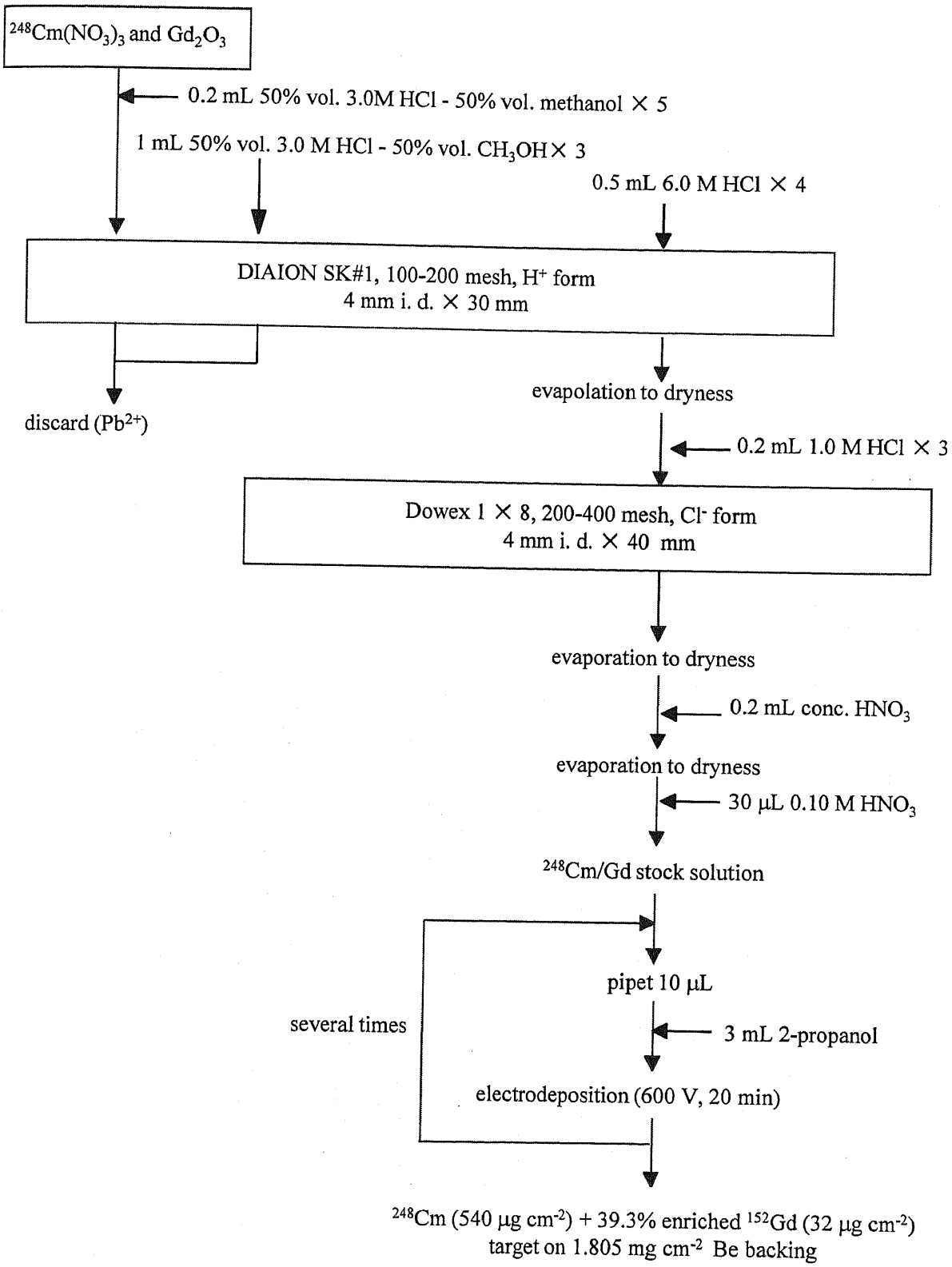

Fig. 2-7. Schematic diagram of the preparation procedure of the Cm/Gd target.

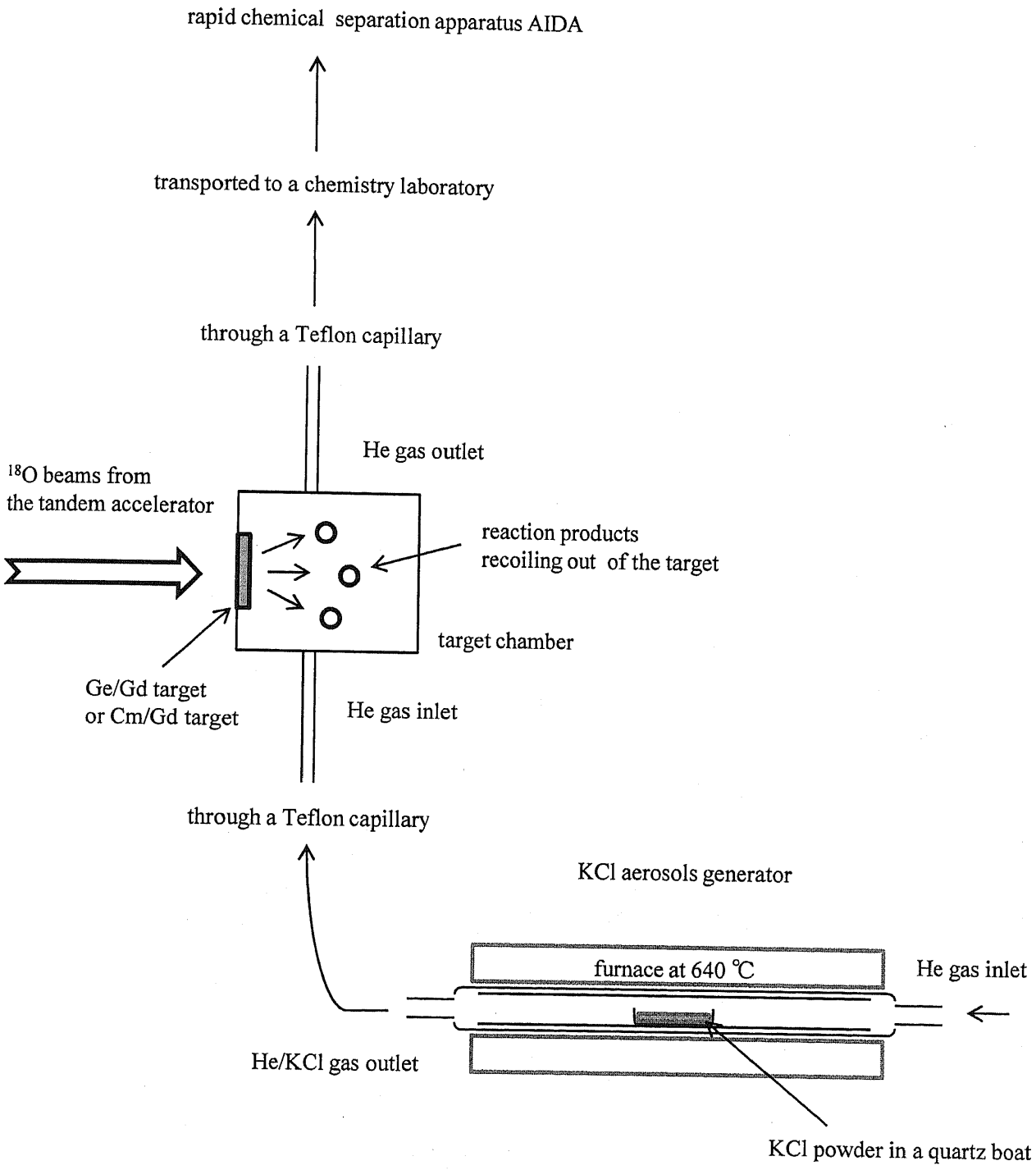

Fig. 2-8. Schematic diagram of the He/KCl gas-jet system.

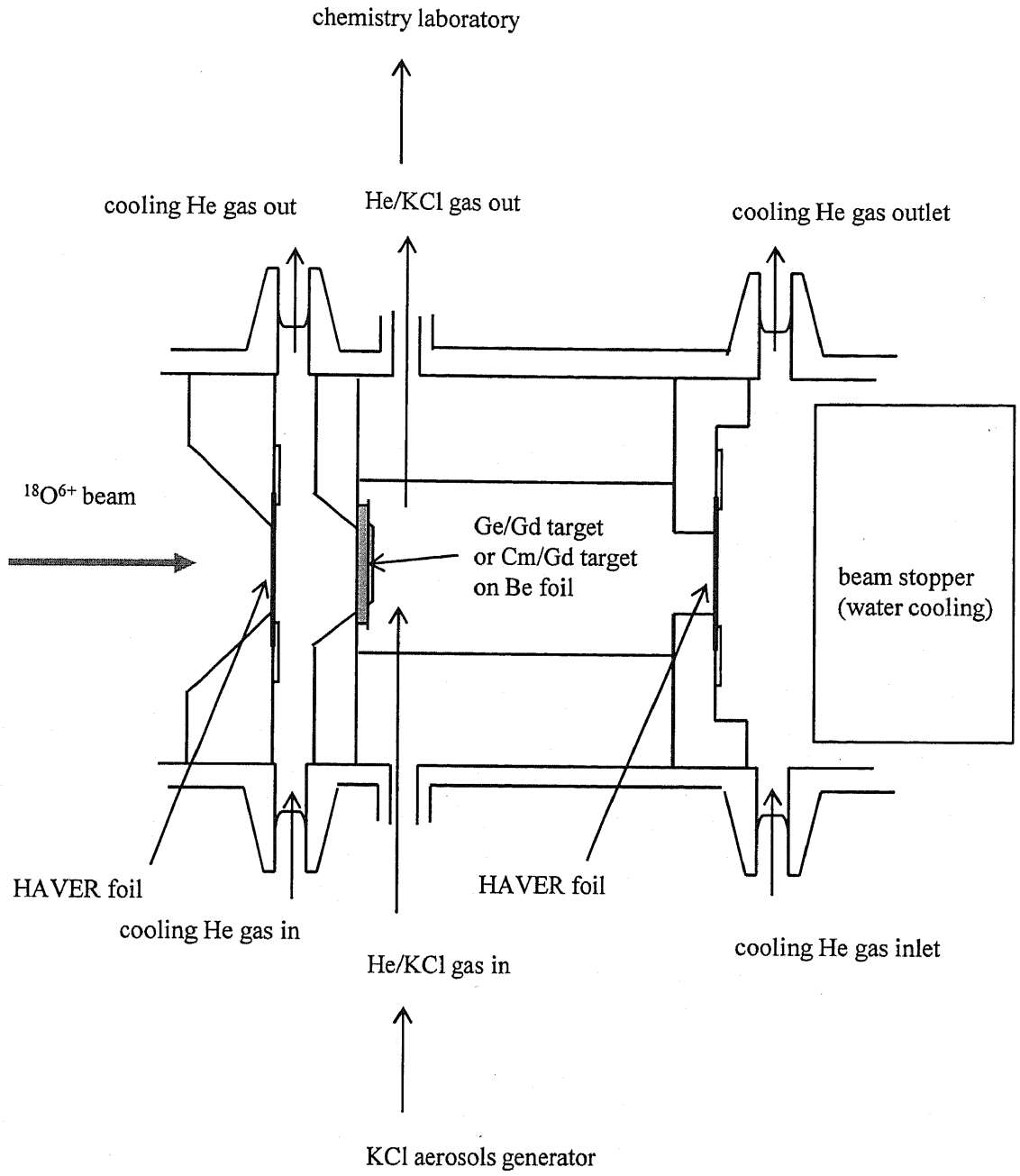

Fig. 2-9. Sectional view of the target chamber.

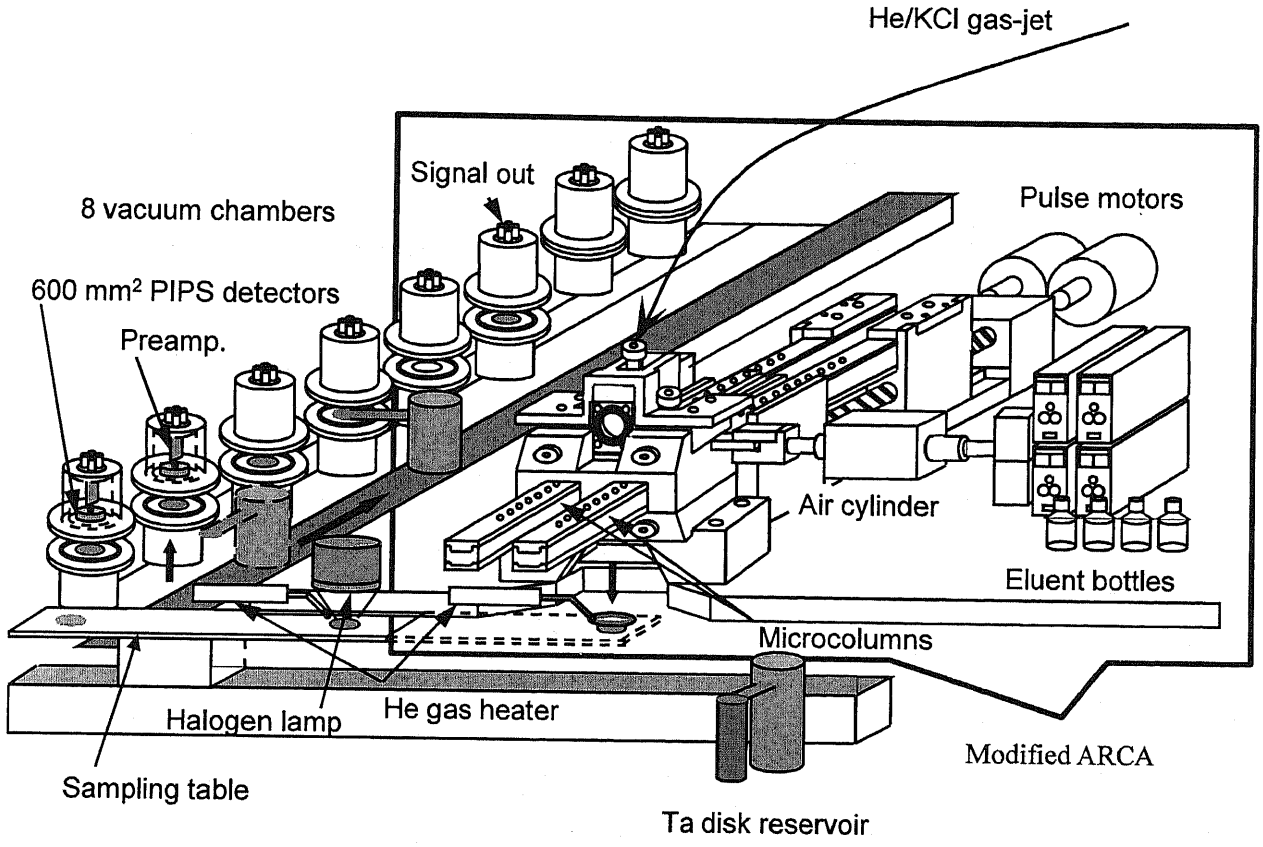

Fig. 2-10. Schematic view of AIDA.

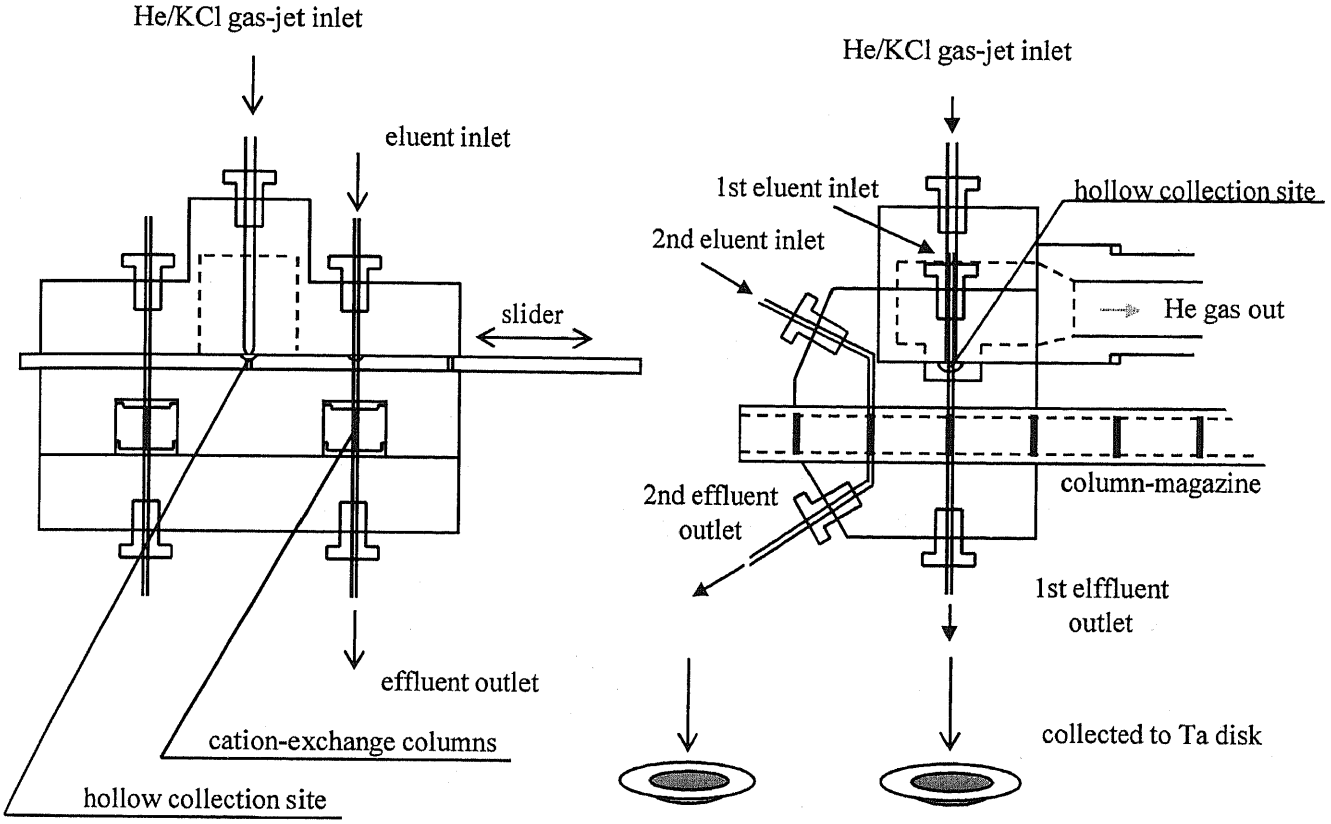

Fig. 2-11. Sectional view of the modified ARCA.

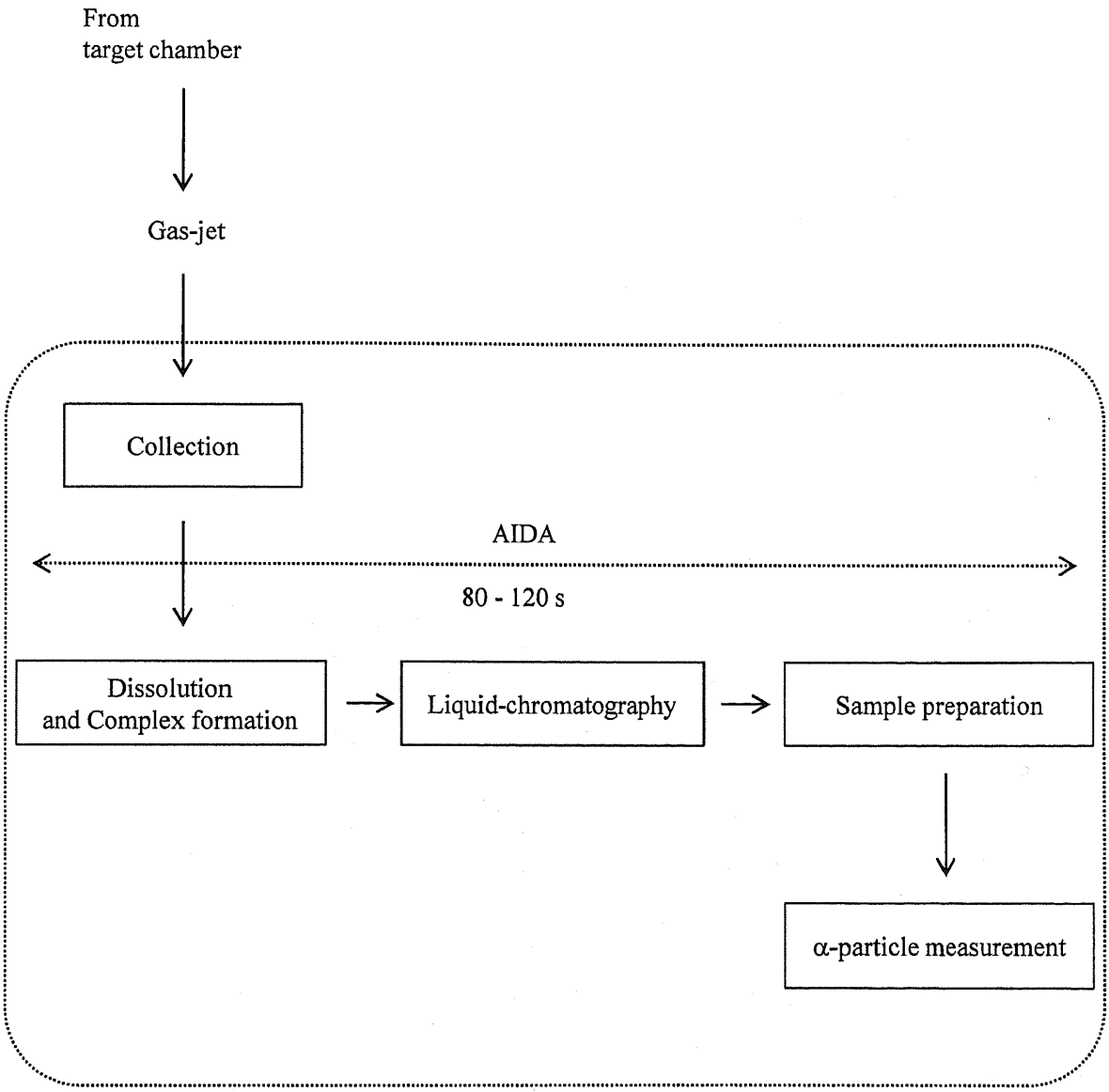

Fig. 2-12. Schematic flow diagram of the liquid chromatographic experiment with Rf.

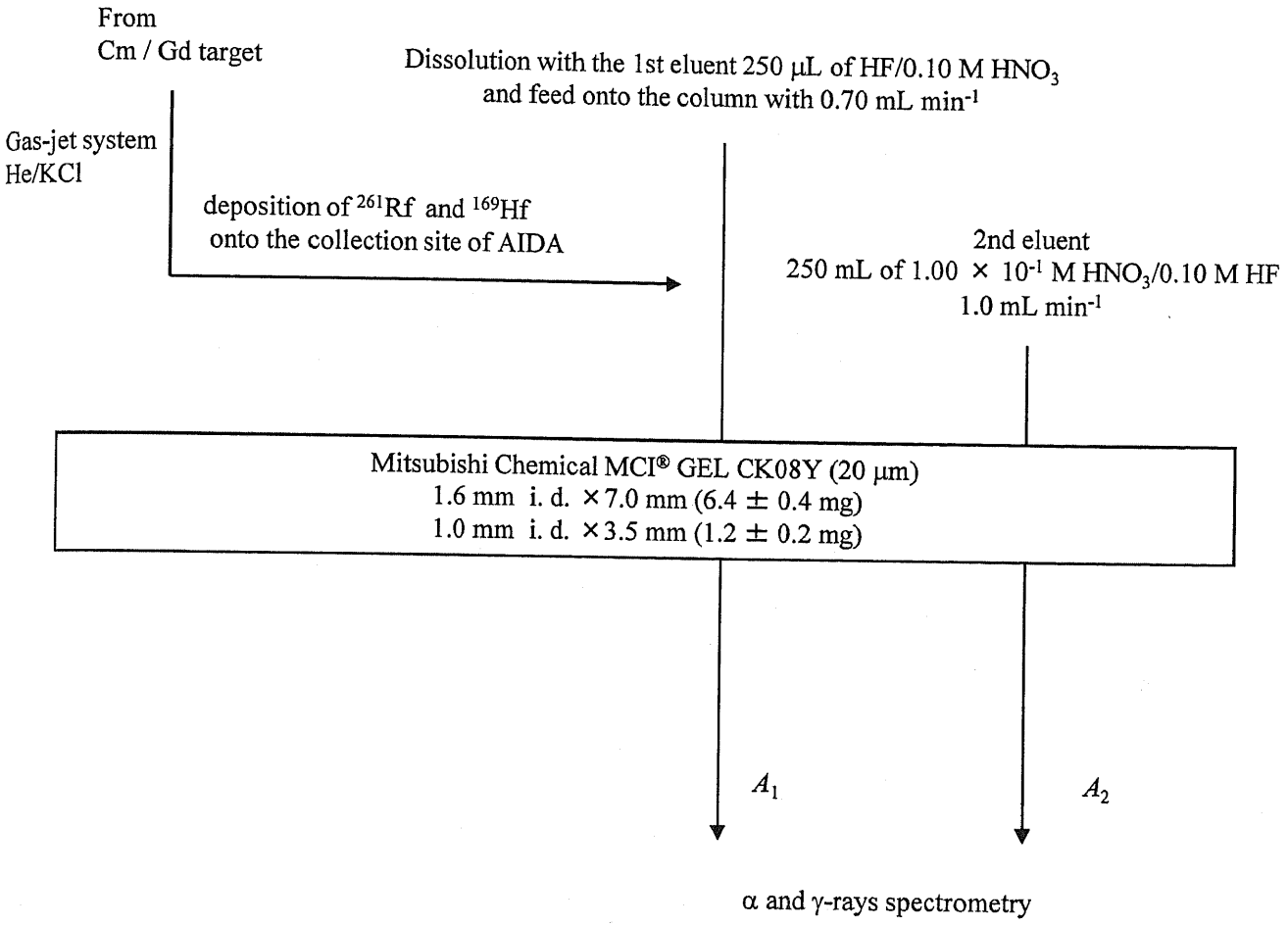

Fig. 2-13. Schematic diagram of the cation-exchange chromatographic method for the Rf experiment.

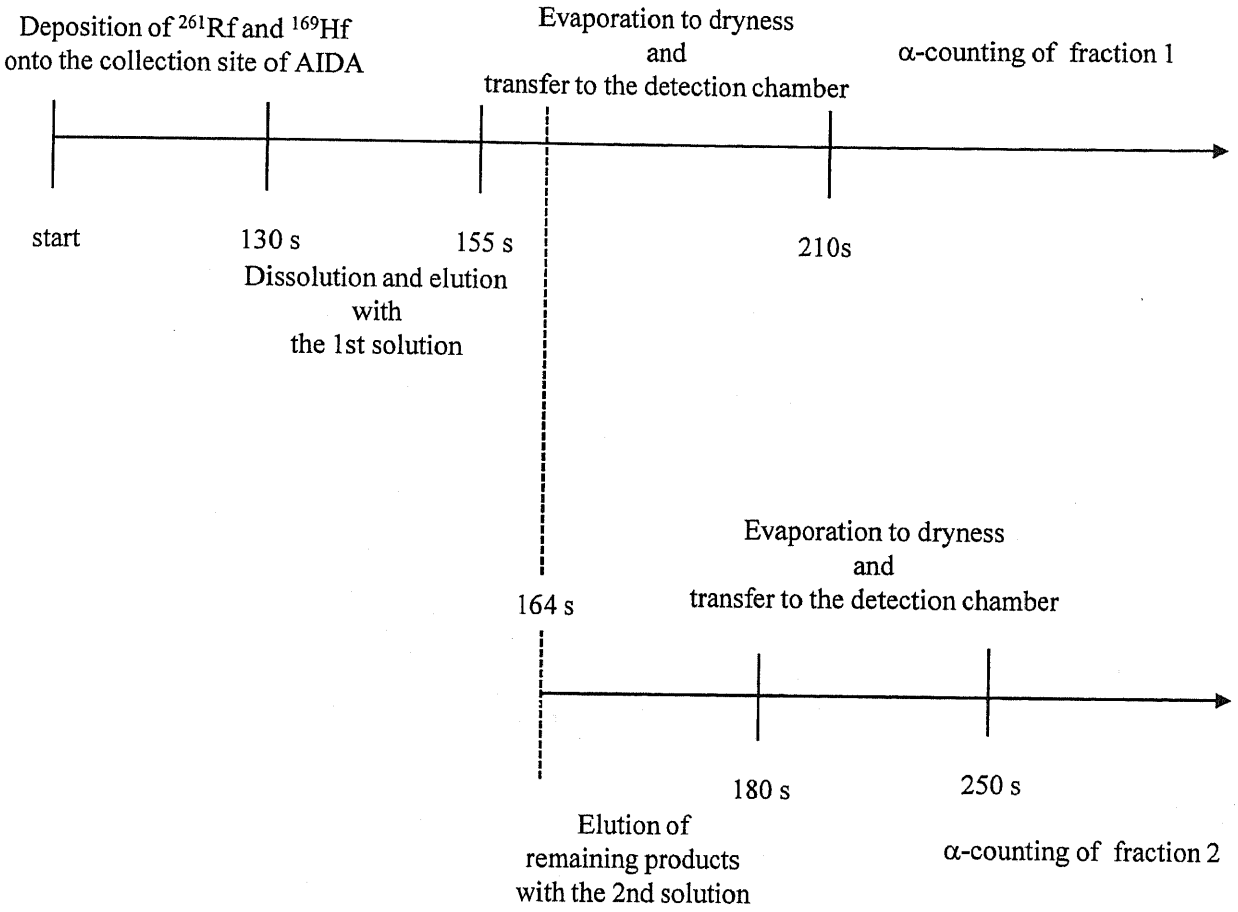

Fig. 2-14. Typical time sequence of the cation-exchange chromatographic method of the Rf experiment.

Chapter 3

Results and discussions

3-1. Variation of distribution coefficients of Rf, Zr, Hf and Th as a function of [F^-] in HF/0.1 M HNO_3

3-1-1. Distribution coefficients of ^{88}Zr, ^{175}Hf and ^{234}Th by batch experiments

Cation-exchange behavior of chemical species between the solution and the resin phases is expressed by the distribution coefficient, K_d (mL g^{-1}) that is given by the following equation,

$$K_d = \frac{A_{Resin} / W_{Resin}}{A_{Solution} / V_{Solution}}, \quad (3\text{-}1)$$

where A_{Resin} and $A_{Solution}$ are the radioactivities of ions in the resin and the solution phases, respectively, and W_{Resin} is the mass of the dry resin (g) and $V_{Solution}$ is the volume of the aqueous solution (mL).

Since the weak acid HF partially dissociates in aqueous solution, the following equilibria are formed in the HF/HNO_3 mixed solution,

$$H^+ + F^- \overset{K_1}{\rightleftharpoons} HF \quad (3\text{-}2)$$

$$HF + F^- \overset{K_2}{\rightleftharpoons} HF_2^- \quad (3\text{-}3)$$

$$HNO_3 \rightleftharpoons H^+ + NO_3^-, \quad (3\text{-}4)$$

with the dissociation constants of K_1 = 935 M^{-1} and K_2 = 3.12 M^{-1} for Eqs. (3-2) and (2-3), respectively [30]. Complete dissociation of the nitric acid was assumed in the present study. So, equilibrated concentrations of each ion in the HF/HNO_3 solution were evaluated on the basis of the law of mass action.

The measured K_d values of ^{88}Zr, ^{175}Hf and ^{234}Th in the HF/0.10 M HNO_3 solutions obtained by the batch experiments are shown as a function of the fluoride ion concentration [F^-]

in Fig. 3-1 and these are listed in Tables 3-1 (Zr and Hf) and 3-2 (Th). The errors were evaluated from the standard deviations in γ-ray counting. The K_d values of these elements are decreased with increasing [F^-]. This feature, as being reported for the determination of the stability constants of fluoro complexes of these elements [31-33], shows the consecutive formation of the fluoro complexes.

The K_d values of Zr and Hf decrease in the lower fluoride ion concentration than those of Th. The adsorption strength on the cation-exchange resin is reduced by the fluoride complexation of these elements. Table 3-3 shows the stability constants β_n of the fluoro complexes of Zr^{4+}, Hf^{4+} and Th^{4+} in HF/4 M $HClO_4$ [30]. It indicates that the strength of the fluoride complexation of Zr and Hf are stronger than that of Th. The present results are well explained by the difference of the stability constants in Table 3-3 and are consistent with the trends observed in Refs. 18 and 19.

3-1-2. Distribution coefficients of ^{85}Zr and ^{169}Hf by on-line experiments

Figures 3-2 and 3-3 show the typical elution curves of ^{85}Zr and ^{169}Hf in HF/0.10 M HNO_3 solutions using the microcolumns of 1.6 mm i.d. × 7.0 mm and 1.0 mm i.d. × 3.5 mm, respectively. The radioactivity per unit volume indicates the percentage of the radioactivity to the totally eluted one per unit volume. According to the Glueckauf model of chromatography [21] which is based on the theoretical plate concept assuming a continuous flow and the local equilibrium, the percent radioactivity per unit volume $A(v)$ with the eluent volume v is represented as

$$A(v) = A_{max} \exp\left\{-\frac{N}{2}\frac{(V_{max}-v)^2}{V_{max}v}\right\}, \qquad (3\text{-}5)$$

where A_{max}, N and V_{max} are the maximum peak height, the number of the theoretical plates and

the effluent volume at the maximum peak height of the elution curve, respectively. It is noted that the value of V_{max} and v are corrected for the dead volume of the columns which are 21 μL and 42 μL for the experiments with the 1.0 mm i. d. × 3.5 mm and 1.6 mm i. d. × 7.0 mm columns, respectively. The results of the fit by Eq. 3-5 are shown in Figs. 3-2 and 3-3 by solid lines and dashed lines for ^{85}Zr and ^{169}Hf, respectively. The fits are in good agreement with the experimental data. The number of theoretical plates N are evaluated to be 7.3 ± 2.8 and 3.0 ± 1.4 for the 1.6 mm i. d. × 7.0 mm and 1.0 mm i. d. × 3.5 mm columns, respectively.

The K_d value based on the column chromatographic method is described as

$$K_d = V_{max} / W_{Resin}. \quad (3\text{-}6)$$

The average W_{Resin} values were measured to be 6.4 ± 0.4 mg and 1.2 ± 0.2 mg for the 1.6 mm i. d. × 7.0 mm and 1.0 mm i. d. × 3.5 mm columns, respectively. The K_d values obtained from the column chromatographic method are plotted in Fig. 3-4. As shown in Fig. 3-4, both K_d values obtained by the batch and the column methods agree well with each other, which indicates that the chemical reactions under the given conditions of the column method reach equilibrium.

3-1-3. Distribution coefficients of ^{261}Rf in HF/0.10 M HNO_3

The results on the Rf experiment are summarized in Table 3-4. A total of 1327 cycles of the cation-exchange experiments were conducted and 147 α-particles from the decays of ^{261}Rf (E_α = 8.28 MeV) [35] and its daughter nuclide ^{257}No (E_α = 8.22 and 8.32 MeV) [36] including 22 α-α correlation events from ^{261}Rf and ^{257}No were observed in the α-particle energy range of 8.00 - 8.36 MeV. The typical α-particle spectra of samples prepared from the two effluents, fractions 1 and 2, in 2.50 × 10^{-2} M HF/0.10 M HNO_3 from the 278 cycles of the experiments are shown in Fig. 3-5. The event ratio of α-singles to α-α correlated pairs was estimated by taking into account the counting efficiency of the detector and the growth and

decay of ^{261}Rf and ^{257}No. The contribution of the α-decay of ^{257}No formed from ^{261}Rf during the collection before the cation-exchange experiment was also taken into account on the basis of the standard equations of growth and decay. It was assumed that the divalent state of ^{257}No [37] was strongly adsorbed on the cation-exchange resin and not eluted with any solutions used in this experiment. Initial number of ^{261}Rf at the collection site, N^0_{Rf}, is disintegrated by α-decay during collection and ion-exchange process,

$$N^0{}_{Rf} = N_{Rf,1} \times \frac{1}{e^{-\lambda_{Rf} t_{ion-exchange}}}, \tag{3-7}$$

where $N_{Rf,1}$ is a number of ^{261}Rf after ion-exchange process, λ_{Rf} is a decay constant of ^{261}Rf and $t_{ion-exchange}$ is the time interval between the start of the sample collection and the end of the ion-exchange process. The growth and decay of ^{261}Rf and ^{257}No is estimated by the equations,

$$N_{Rf,2} = N_{Rf,1} e^{-\lambda_{Rf} t} \tag{3-8}$$

$$N_{No} = \frac{\lambda_{Rf}}{\lambda_{No} - \lambda_{Rf}} N_{Rf,2} (e^{-\lambda_{Rf} t} - e^{-\lambda_{No} t}) \tag{3-9}$$

where λ_{No} is a decay constant of ^{257}No, and $N_{Rf,2}$ and N_{No} are numbers of ^{261}Rf and ^{257}No after cooling time t, respectively. Using Eqs. 3-8 and 3-9, numbers of decayed ^{261}Rf and ^{257}No during the counting time are

$$\int_{t_s}^{t_e} A_{Rf} dt = \int_{t_s}^{t_e} \lambda_{Rf} N_{Rf,1} e^{-\lambda_{Rf} t} dt = N_{Rf,1} (e^{-\lambda_{Rf} t_s} - e^{-\lambda_{Rf} t_e}), \tag{3-10}$$

$$\int_{t_s}^{t_e} A_{No} dt = \int_{t_s}^{t_e} \lambda_{No} N_{No} dt = \int_{t_s}^{t_e} \frac{\lambda_{Rf}}{\lambda_{No} - \lambda_{Rf}} N_{Rf,2} (e^{-\lambda_{Rf} t} - e^{-\lambda_{No} t}) dt$$

$$= \frac{N_{Rf}}{\lambda_{No} - \lambda_{Rf}} \{(e^{-\lambda_{Rf} t_s} - e^{-\lambda_{Rf} t_e}) \lambda_{No} + (e^{-\lambda_{No} t_s} - e^{-\lambda_{No} t_e}) \lambda_{Rf}\}, \tag{3-11}$$

where A_{Rf} and A_{No} are radioactivities of ^{261}Rf and ^{257}No, respectively, t_s is the elapsed time between the midpoint during the ion-exchange process and the start of the α-counting, and t_e is

the elapsed time between the midpoint during the ion-exchange process and the end of the α-counting. By taking into account the counting efficiency of the detector (35%), the event ratio of α-singles to α-α correlated pairs is estimated to be 5.0. The observed ratio of 4.8 ± 1.7 is consistent with the estimated value within a statistical error. The average background counts were determined in a long counting interval after the Rf experiment. It was 3.2×10^{-6} counts s^{-1} for each detector in the α-particle energy range of interest.

The K_d values of Rf were evaluated from percent adsorption (%ads) values at 250 μL of eluent by assuming that the reaction kinetics in the fluoride complexation and cation-exchange processes of Rf are as fast as those for Zr and Hf. Figure 3-6 shows the variations of the %ads values of Zr and Hf on the cation-exchange resin CK08Y obtained with the microcolumns, 1.6 mm i. d. × 7.0 mm and 1.0 mm i. d. × 3.5 mm, as a function of the distribution coefficients K_d obtained by the batch method. The correlation between the %ads values and the K_d values was fitted by a following equation containing the free parameters *a*, *b* and *c*,

$$\%\text{ads} = 100\exp[-a\exp\{-b(K_d - c\}] \ . \qquad (3\text{-}12)$$

The fitting values based on Eq. 3-12 are shown by the solid curves in Fig. 3-6 for each microcolumn. The %ads values of Rf from the column method can be transformed into the K_d values using this relationship. The asymmetric error limits of the %ads values of ^{261}Rf were evaluated from the counting statistics of the observed α events based on the 68% confidence intervals for Poisson distributed variables [38].

In general, a probability distribution of independent discrete variables, such as digital counting of radiation, is described by Poisson distribution *P*,

$$P(x|\mu) = \frac{\mu^x}{X!}e^{-\mu}, \qquad (3\text{-}13)$$

where the parameters μ and X are the population mean (equal to population variance) and the sample mean, respectively. Especially if the μ is large, Poisson distribution approaches to symmetric Gaussian distribution and the standard deviation σ (a square root of population variance) is approximated by a root of X. In the observation of rare event, however, because probability distribution of Poisson distribution is asymmetric, the representation instead of the standard deviation is needed. Equation 3-13 represents the distribution of the probability of the number of the observed events X with the known population mean μ. Here, it is needed to estimate population mean μ with the known number of the observed events X. The probability, $P(x)$, that each of population mean μ gives the number of observed events X, is represented by a following equation,

$$P(\mu|x) = \frac{\int_{\mu_l}^{\mu_u} P(x|\mu)d\mu}{P_{prior}} , \qquad (3\text{-}14)$$

where P_{prior} is a normalization factor which is set to 1 because none of the possible value is excluded and μ_l and μ_u are lower and upper limits, respectively. Although Poisson distribution is discrete, the probability as a function of μ is continuous because μ can take integer or real values. A background from contamination, such as electronic noise and/or cosmic rays is considered. Some of the number of average background has larger than that of the observed events, resulting in the negative number of the corrected events. Therefore, a weighted actual background is obtained by re-normalizing Poisson distribution of the number of background events to 100% between zero and X and averaging the re-normalized values. Each of the probability of population mean μ against the corrected value is evaluated in a same way as mentioned above.

Figure 3-7 shows the K_d values of Zr, Hf, Th and Rf on the cation-exchange resin (CK08Y) in 0.1 M HNO_3 depending on the concentration of [F^-]. It is clearly found that the K_d values of Rf also decrease with an increase of [F^-] and lie between those of Zr/Hf and Th. The

present results indicate that the fluoride complex formation of Rf successively proceeds in the same way as for the homologues. Further, it suggests that the fluoride complexation of Rf is significantly weaker than that of Zr and Hf, but it would be stronger than the complexation of Th.

3-2. Variation of distribution coefficients of Rf, Zr, Hf and Th as a function of $[H^+]$ in HF/HNO_3

3-2-1. Distribution coefficients of ^{88}Zr, ^{175}Hf and ^{234}Th in $\log K_d$ vs. $\log[H^+]$

Figures 3-8 and 3-9 show the variation of the K_d values of ^{88}Zr and ^{175}Hf, and ^{234}Th, respectively, at various fluoride ion concentrations $[F^-]$ using the batch method. It is found that the $\log K_d$ of these elements are linearly decrease with an increases of $\log[H^+]$. The solid and dashed lines in Fig. 3-8 are the results of the least squares fitting to the data of Zr and Hf, respectively. Figure 3-10 shows the variation of the slopes for ^{88}Zr, ^{175}Hf and ^{234}Th in the $\log K_d$ vs. $\log[H^+]$ plot as a function of $[F^-]$. The slope values were obtained by the least squares fitting method. As shown in Fig. 3-10, it is regarded that the slopes of these ions show a constant value of about -2.5 at $[F^-] > 10^{-6}$ M; the slopes for each element are independent of the fluoride ion concentration above $[F^-] \sim 10^{-6}$ M.

At the constant fluoride ion concentration, cation-exchange behavior of cationic fluoro complexes between the solution and the cation-exchange resin phases is expressed by the following reaction,

$$(4-n_R)H^+ + MF_{n_R}{}^{(4-n_R)+}{}_{Resin} \rightleftharpoons (4-n_R)H^+{}_{Resin} + MF_{n_R}{}^{(4-n_R)+}, \qquad (3\text{-}15)$$

where n_R is the average number of the coordinated fluoride ions to M^{4+} on the cation-exchange

resin,

$$n_R = \frac{\left([MF^{3+}]_{Resin} + 2[MF_2^{2+}]_{Resin} + 3[MF_3^{+}]_{Resin} \cdots\right)}{\left([MF^{3+}]_{Resin} + [MF_2^{2+}]_{Resin} + [MF_3^{+}]_{Resin} \cdots\right)}, \tag{3-16}$$

Introducing the selectivity coefficient K,

$$K = \left([H^+]_{Resin}^{(4-n_R)} \cdot [MF_{n_R}^{(4-n_R)+}]\right) / \left([H^+]^{(4-n_R)} \cdot [MF_{n_R}^{(4-n_R)+}]_{Resin}\right). \tag{3-17}$$

The distribution coefficient of these cations is expressed,

$$\begin{aligned} K_d &\equiv [MF_{n_R}^{(4-n_R)+}]_{Resin} / [MF_{n_R}^{(4-n_R)+}] \\ &= (1/K)\left([H^+]_{Resin}^{(4-n_R)} / [H^+]^{(4-n_R)}\right) \\ &= (1/K)\left([H^+]_{Resin} / [H^+]\right)^{(4-n_R)}. \end{aligned} \tag{3-18}$$

Transforming both sides of Eq. 3-18 into logarithmic form,

$$\log K_d \propto (4 - n_R) \log\left([H^+]_{Resin} / [H^+]\right). \tag{3-19}$$

Because the concentration of the cationic fluoro complexes is negligibly small compared with those of the hydrogen ion in the solution and the resin phases, $[MF_x^{(4-x)+}] << [H^+]$ and $[MF_x^{(4-x)+}] << [H^+]_{Resin}$, in the tracer scale experiment, $[H^+]_{Resin}$ and K are taken as a constant. Thus, from the slope in the $\log K_d$ vs. $\log[H^+]$ plot, we can evaluate the average number of the coordinated fluoride ions to the metal cation on the cation-exchange resin. At $[F^-] = 0$ M, the slopes of Zr^{4+} and Hf^{4+} are not -4 as shown in Fig. 3-10. In this condition, it is expected that hydrolysis or coordination of the nitrate ion NO_3^- to Zr^{4+} and Hf^{4+} would occur. The slopes obtained at $[F^-] \geq 10^{-6}$ M, are about -2.5. Thus, the average number of the coordinated fluoride ions on the

cation-exchange resin is deduced to be about 1.5. In the present conditions, MF^{3+} and MF_2^{2+} are dominatingly present on the cation-exchange resin. However, the coordination of the dissolved nitrate ion (NO_3^-) would be possible that influences these slopes. To confirm the contribution of the coordination of NO_3^-, the variation of the K_d values of ^{88}Zr and ^{175}Hf, and ^{234}Th were also measured using the less coordinating support electrolyte, the perchlorate ion (ClO_4^-). The slopes obtained in the $HF/HClO_4$ solution are shown in Fig. 3-11. It is found that these slopes at $[F^-] > 10^{-6}$ M are the same as those observed in HF/HNO_3. In this concentration region of the fluoride ion, no effect from the dissolved ion NO_3^- was observed.

3-2-2. Distribution coefficients of ^{261}Rf in logK_d vs. log[H^+]

The K_d values of ^{261}Rf against $[H^+]$ were measured at $[F^-] = 1.06 \times 10^{-4}$ M, because the range of the measurable K_d values with the present AIDA system is limited by the size of the microcolumns to be approximately 20 to 300. The results on the Rf experiment are summarized in Table 3-5. A total of 1001 cycles of the cation-exchange experiment were conducted, and 134 α-particles from the decays of ^{261}Rf and ^{257}No, including 23 α-α correlation events from ^{261}Rf and ^{257}No were observed in the α-particles energy range of 8.00 - 8.36 MeV. The event ratio between α singles and α-α correlations was estimated to be 5.0 by the same method deduced in 3-1-3. The observed ratio of 3.8 ± 0.5 is reasonably consistent with the estimated ratio. The K_d

values of Rf were evaluated by the same method in the HF/0.10 M HNO_3 experiment.

The K_d values of Rf together with those of Zr, Hf and Th at $[F^-] = 1.06 \times 10^{-4}$ M as a function of the hydrogen ion concentration $[H^+]$ are shown in Fig. 3-12. It is found that $\log K_d$ of Rf also linearly decreases with increasing $\log[H^+]$, which implies that the adsorption equilibrium of Rf is dominated by competitive sorption of H^+ in this $[H^+]$ range as those with the homologues. The slope in the $\log K_d$ vs. $\log[H^+]$ plot of Rf is determined to be -2.3 ± 0.4, indicating that the average number of the coordinated fluoride ions to Rf on the cation-exchange resin is deduced to be about 1.5. In the present condition, RfF^{3+} and RfF_2^{2+} are also likely present on the cation-exchange resin as those with Zr, Hf and Th.

3-3. Fluoride complexation of Rf

In the HF/0.10 M HNO_3 solution, the K_d values of Rf decrease with increasing the concentration of the fluoride ion $[F^-]$ as those with the homologues Zr, Hf and Th as shown in Fig. 3-7. It indicates that the fluoride complex formation of Rf successively proceeds in the same way as for the homologues,

$$M^{4+} + F^- \rightleftharpoons MF^{3+}$$

$$MF^{3+} + F^- \rightleftharpoons MF_2^{2+}$$

$$MF_2^{2+} + F^- \rightleftharpoons MF_3^{+}$$

$$MF_3^+ + F^- \rightleftharpoons MF_4$$

$$MF_4 + F^- \rightleftharpoons MF_5^-$$

$$MF_5^- + F^- \rightleftharpoons MF_6^{2-}.$$

The K_d values of Rf also were decreased with increasing the concentration of the hydrogen ion $[H^+]$ as those with the homologues Zr, Hf and Th as shown in Fig. 3-12. It was found that the $\log K_d$ of these elements are linearly decrease with an increase of $\log[H^+]$. From Eq. 3-19 as already mentioned, it was indicated that the cationic fluoro complexes of these elements are replaced with the H^+ ion on the cation-exchange site and the slope in the $\log K_d$ vs. $\log[H^+]$ plot shows the average number of the coordinated fluoride ions to the metal cation on the cation-exchange resin.

The slopes of Zr and Hf in the $\log K_d$ vs. $\log[H^+]$ plot as shown in Fig. 3-10 are varied with the fluoride ion concentration at $[F^-] < 10^{-6}$ M, thus, it is expected that the chemical forms of these ions are changing with the composition of the solution. However, the slopes of those elements show the constant value -2.5 at $[F^-] \geq 10^{-6}$ M. This would mean that the chemical forms of the cationic fluoro complexes of Zr, Hf, Th and Rf are the same on the cation-exchange resin in this $[F^-]$ region. The distribution coefficient of metal ions between the solution and the resin phases is expressed by the following equation,

$$\begin{aligned} K_d &\equiv [MF_{n_R}^{(4-n_R)+}]_{Resin} / [MF_{n_R}^{(4-n_R)+}] \\ &= ([M^{4+}]_{Resin} + [MF^{3+}]_{Resin} + [MF_2^{2+}]_{Resin} + \cdots) / ([M^{4+}] + [MF^{3+}] + [MF_2^{2+}] + \cdots) \\ &= ([M^{4+}]_{Resin} + \beta_{1,R}[M^{4+}]_{Resin}[F^-]_{Resin} + \beta_{2,R}[M^{4+}]_{Resin}[F^-]_{Resin}^2 + \cdots) / \\ &\quad ([M^{4+}] + \beta_1[M^{4+}][F^-] + \beta_2[M^{4+}][F^-]^2 + \cdots) \\ &= [M^{4+}]_{Resin}(1 + \beta_{1,R}[F^-]_{Resin} + \beta_{2,R}[F^-]_{Resin}^2 + \cdots) / [M^{4+}](1 + \beta_1[F^-] + \beta_2[F^-]^2 + \\ &\quad \cdots), \end{aligned} \tag{3-20}$$

where $\beta_{n,R}$ and β_n are stability constants of the fluoride complexation in the resin and the solution phases, respectively. As the slopes of each ion of Zr, Hf and Th are constant in $[F^-] \geq 10^{-6}$ M, it would be suggested that the fluoride ion concentration in the vicinity of the resin site is not altered by change of $[F^-]$. This means that the fluoride ion concentration in the resin phase is saturated because the anionic fluoride ion hardly exists on the site of the cation-exchange resin electrostatically. On the other hand, the stability constants of the fluoride complexation of Zr^{4+}, Hf^{4+} and Th^{4+} in the resin phase should affect the slopes of these ions, although no significant difference in the slopes is seen as depicted in Figs. 3-10 and 3-11.

As mentioned above the slopes of those elements show a constant value -2.5 in $[F^-] \geq 10^{-6}$ M. It is assumed that the observed difference of the adsorption of these ions depends on the chemical forms of fluoro complexes in the solution phase (see Fig. 3-13) and/or the electrostatic density of fluoro ions in the resin phase. From the former assumption, the order of the adsorption strength of these ions at the same $[F^-]$ is expected to be Th > Zr ~ Hf, while from the latter assumption, the sequence is expected to be Zr ~ Hf > Th, because the cationic densities deduced from the ionic radii (IR) of these tetravalent ions are expected to be Zr (72 pm) < Hf (71 pm) << Th (94 pm) (see Ref. 39 for Zr, Hf and Th). Thus, the adsorption strength of these ions strongly depends on the chemical forms of the fluoro complexes in the solution phase under the present experimental conditions.

According to the hard and soft acids and bases concept (HSAB) [40,41], Rf is expected to be classified as the hard acid as same as Zr, Hf and Th based on the observation of the strong interaction with the hard base of the fluoride ion. The hard acid - hard base type metal fluoro complexes serve as good models for the ionic and electrostatic interaction between metal cations and the fluoride ions. The fluoride complexation strongly depends on the electronic density of the metal cations that originates from the size of the metal cations. Thus, a correlation between

the ionic radii (IR) and the strengths of the fluoride complexation (K_d) is expected, which is valid only for the adsorption of cationic complexes. The IRs of these elements vary in the order of Zr (72 pm) ~ Hf (71 pm) < Rf (76 pm) [7] << Th (94 pm). This trend shows the reverse order of the strength of the fluoride complexation experimentally obtained. The present result clearly indicates the size of Rf^{4+} would be in between those of Zr^{4+} and Hf^{4+}, and Th^{4+}.

Table 3-1. K_d-values of Zr and Hf on the cation-exchange resin (CK08Y) in HF/0.10 M HNO_3 at various HF concentrations.

[HF] / M	[F^-] / M	$K_d(^{85}Zr)$ / mL g^{-1}	$K_d(^{175}Hf)$ / mL g^{-1}
1.00×10^{-4}	1.06×10^{-6}	3130 ± 150	6680 ± 430
3.00×10^{-4}	3.17×10^{-6}	705 ± 21	1260 ± 30
5.00×10^{-4}	5.29×10^{-6}	276 ± 9	394 ± 10
5.50×10^{-4}	5.82×10^{-6}	195 ± 3	311 ± 9
6.00×10^{-4}	6.35×10^{-6}		258 ± 6
6.50×10^{-4}	6.88×10^{-6}	148 ± 2	227 ± 7
7.00×10^{-4}	7.41×10^{-6}	124 ± 4	190 ± 5
7.50×10^{-4}	7.94×10^{-6}	104 ± 2	160 ± 5
8.50×10^{-4}	8.99×10^{-6}	82.2 ± 3.5	129 ± 4
1.00×10^{-3}	1.06×10^{-5}	61.1 ± 2.7	82.6 ± 2.9
1.10×10^{-3}	1.16×10^{-5}	43.3 ± 0.7	61.3 ± 2.0
1.25×10^{-3}	1.32×10^{-5}	36.3 ± 2.1	51.4 ± 2.4
1.40×10^{-3}	1.48×10^{-5}	26.8 ± 0.4	34.6 ± 1.1
1.80×10^{-3}	1.90×10^{-5}	14.4 ± 0.2	18.8 ± 0.7
2.00×10^{-3}	2.12×10^{-5}	10.9 ± 1.5	13.6 ± 2.0
2.50×10^{-3}	2.64×10^{-5}	7.99 ± 0.78	8.44 ± 1.14
3.00×10^{-3}	3.17×10^{-5}	5.43 ± 0.69	6.11 ± 1.69
4.00×10^{-3}	4.23×10^{-5}	2.61 ± 0.35	2.30 ± 0.67
5.00×10^{-3}	5.29×10^{-5}	1.74 ± 0.33	0.92 ± 0.65
6.00×10^{-3}	6.34×10^{-5}	0.84 ± 0.34	0.96 ± 0.33
7.00×10^{-3}	7.40×10^{-5}	0.07 ± 0.32	0.36 ± 0.16
8.50×10^{-3}	8.98×10^{-5}	0.67 ± 0.33	0.12 ± 0.16

Table 3-2. K_d-values of Th on the cation-exchange resin (CK08Y) in HF/0.10 M HNO_3 at various HF concentrations.

[HF] / M	[F^-] / M	$K_d(^{234}Th)$ / mL g^{-1}
0.00600	6.34×10^{-5}	6810 ± 220
0.0100	1.06×10^{-4}	5550 ± 7
0.0125	1.32×10^{-4}	1800 ± 60
0.0200	2.11×10^{-4}	751 ± 19
0.0400	4.20×10^{-4}	174 ± 6
0.0500	5.24×10^{-4}	137 ± 5
0.0700	7.31×10^{-4}	63.0 ± 2.9
0.100	1.04×10^{-4}	38.4 ± 4.0
0.125	1.29×10^{-4}	26.9 ± 1.0
0.200	2.02×10^{-3}	6.57 ± 1.01
0.500	4.62×10^{-3}	0.83 ± 0.37
1.00	7.75×10^{-3}	0.06 ± 0.37
2.00	1.13×10^{-3}	0.22 ± 0.40

Table 3-3. Stability constants of the fluoro complexes of Zr^{4+}, Hf^{4+} and Th^{4+} in HF /4 M $HClO_4$ [34].

	Zr^{4+}	Hf^{4+}	Th^{4+}
$\log\beta_1$	9.44	9.03	8.21
$\log\beta_2$	17.23	16.56	14.72
$\log\beta_3$	23.8	23.1	18.6
$\log\beta_4$	29.5	28.7	23.2
$\log\beta_5$	34.6	34.0	-
$\log\beta_6$	38.4	38.0	-

$M^{4+} + nF^- \rightleftharpoons MF_n^{(4-n)+}$ $\beta_n = [MF_n^{(4-n)+}]/[M^{4+}][F^-]^n$

Table 3-4. Summary of the on-line experiments of Rf in HF/0.10 M HNO_3 solutions.

[HF] / M	[HNO_3] / M	[F^-] / M	Column size	Beam dose / $\times 10^{17}$	Number of cycles of the experiment	α-count in Fraction 1		α-count in Fraction 2	
						α	α–α	α	α–α
5.00×10^{-3}	0.10	5.29×10^{-5}	1.0 mm i. d. × 3.5 mm	0.497	251	2	0	23	2
1.00×10^{-2}	0.10	1.06×10^{-4}	1.0 mm i. d. × 3.5 mm	1.02	429	32	4	12	0
1.30×10^{-2}	0.10	1.37×10^{-4}	1.0 mm i. d. × 3.5 mm	0.254	108	7	1	3	0
2.50×10^{-2}	0.10	2.63×10^{-4}	1.6 mm i. d. × 7.0 mm	0.667	278	25	5	17	4
4.00×10^{-2}	0.10	4.20×10^{-4}	1.6 mm i. d. × 7.0 mm	0.193	82	16	4	0	0
1.00×10^{-1}	0.10	1.04×10^{-3}	1.6 mm i. d. × 7.0 mm	0.257	179	10	2	0	0

[HF] / M	[HNO_3] / M	[F^-] / M	Column size	%ads of ^{261}Rf / %	K_d vale of ^{261}Rf / mL g^{-1}
5.00×10^{-3}	0.10	5.29×10^{-5}	1.0 mm i. d. × 3.5 mm	$95.6^{+98.5}_{-90.9}$	315^{+85}_{-58}
1.00×10^{-2}	0.10	1.06×10^{-4}	1.0 mm i. d. × 3.5 mm	$36.7^{+45.4}_{-29.4}$	104^{+19}_{-24}
1.30×10^{-2}	0.10	1.37×10^{-4}	1.0 mm i. d. × 3.5 mm	$39.2^{+57.1}_{-26.3}$	100^{+50}_{-29}
2.50×10^{-2}	0.10	2.63×10^{-4}	1.6 mm i. d. × 7.0 mm	$50.1^{+59.2}_{-43.7}$	$25^{+1.6}_{-1.7}$
4.00×10^{-2}	0.10	4.20×10^{-4}	1.6 mm i. d. × 7.0 mm		
1.00×10^{-1}	0.10	1.04×10^{-3}	1.6 mm i. d. × 7.0 mm		

Table 3-5. Summary of the on-line experiments of Rf in HF/ HNO_3 solutions.

[HF] / M	$[H^+]$ / M	$[F^-]$ / M	Column size	Beam dose / $\times 10^{17}$	Number of cycles of the experiment	α-count in Fraction 1		α-count in Fraction 2	
						α	α–α	α	α–α
7.06×10^{-2}	0.070	1.06×10^{-4}	1.0 mm i.d. × 3.5 mm	0.507	215	3	0	22	5
1.00×10^{-2}	0.10	1.06×10^{-4}	1.0 mm i.d. × 3.5 mm	1.02	429	32	4	12	0
1.25×10^{-2}	0.125	1.06×10^{-4}	1.0 mm i.d. × 3.5 mm	0.280	119	13	3	3	0
1.75×10^{-2}	0.175	1.06×10^{-4}	1.6 mm i.d. × 7.0 mm	2.87	119	1	0	20	3
2.24×10^{-2}	0.225	1.06×10^{-4}	1.6 mm i.d. × 7.0 mm	0.394	116	17	5	11	3

[HF] / M	$[H^+]$ / M	$[F^-]$ / M	Column size	%ads of ^{261}Rf / %	K_d vale of ^{261}Rf / mL g^{-1}
7.06×10^{-2}	0.070	1.06×10^{-4}	1.0 mm i.d. × 3.5 mm	$92.2^{+96.3}_{-86.8}$	320^{+80}_{-63}
1.00×10^{-2}	0.10	1.06×10^{-4}	1.0 mm i.d. × 3.5 mm	$36.7^{+45.4}_{-29.4}$	104^{+19}_{-24}
1.25×10^{-2}	0.125	1.06×10^{-4}	1.0 mm i.d. × 3.5 mm	$24.7^{+38.5}_{-15.0}$	60^{+32}_{-26}
1.75×10^{-2}	0.175	1.06×10^{-4}	1.6 mm i.d. × 7.0 mm	$97.2^{+99.5}_{-97.2}$	30^{+20}_{-10}
2.24×10^{-2}	0.225	1.06×10^{-4}	1.6 mm i.d. × 7.0 mm	$48.7^{+48.8}_{-39.9}$	$24^{+2.5}_{-0.8}$

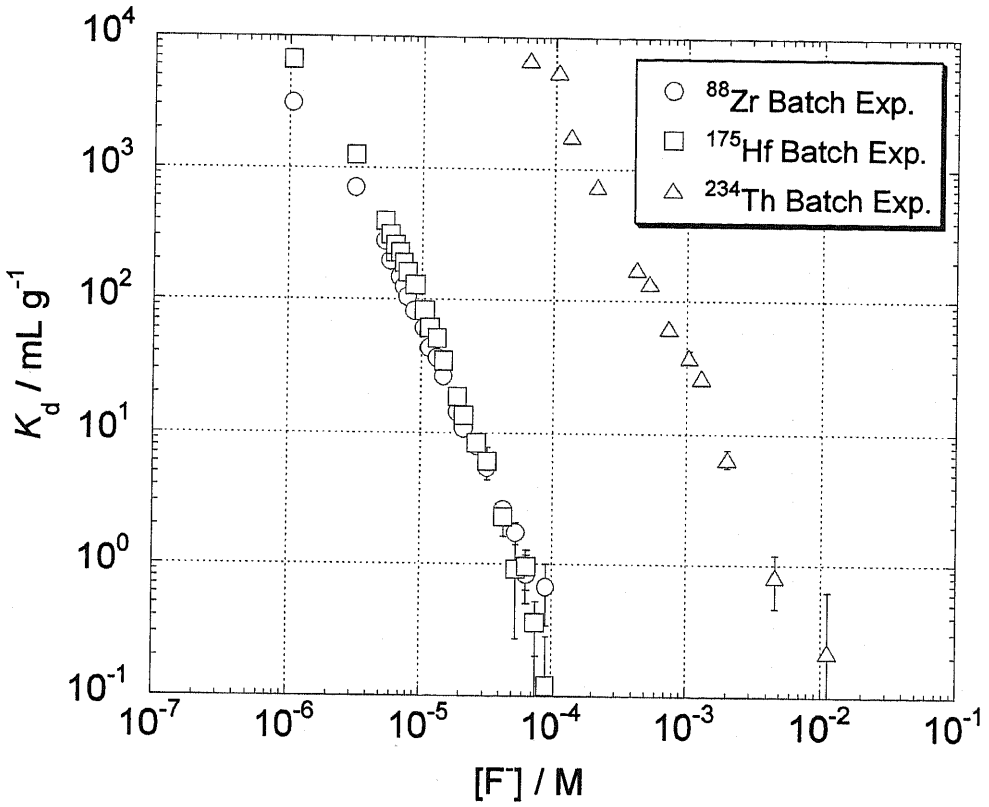

Fig. 3-1. Adsorption behavior of Zr, Hf and Th on cation-exchange resin (CK08Y) in HF/0.10 M HNO_3 at various HF concentrations. The data are obtained by the batch method.

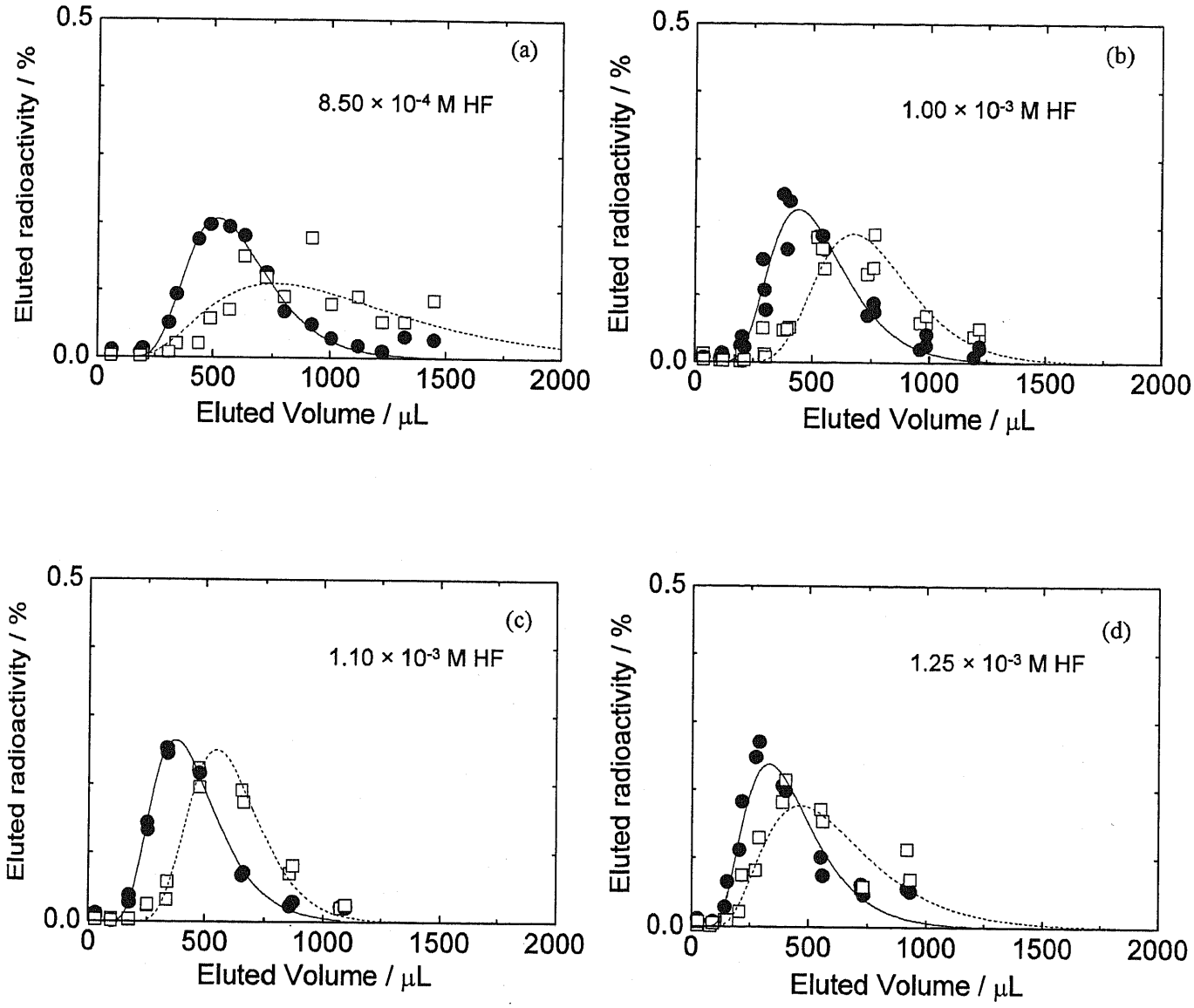

Fig. 3-2. Elution curves of ^{85}Zr and ^{169}Hf in HF/0.10 M HNO_3 solutions with the 1.6 mm i. d. × 7.0 mm columns, ●: Zr and □: Hf. The concentrations of HF are indicated in each figures. The solid and dashed lines indicate the results of the fits by the Glueckauf equation [21].

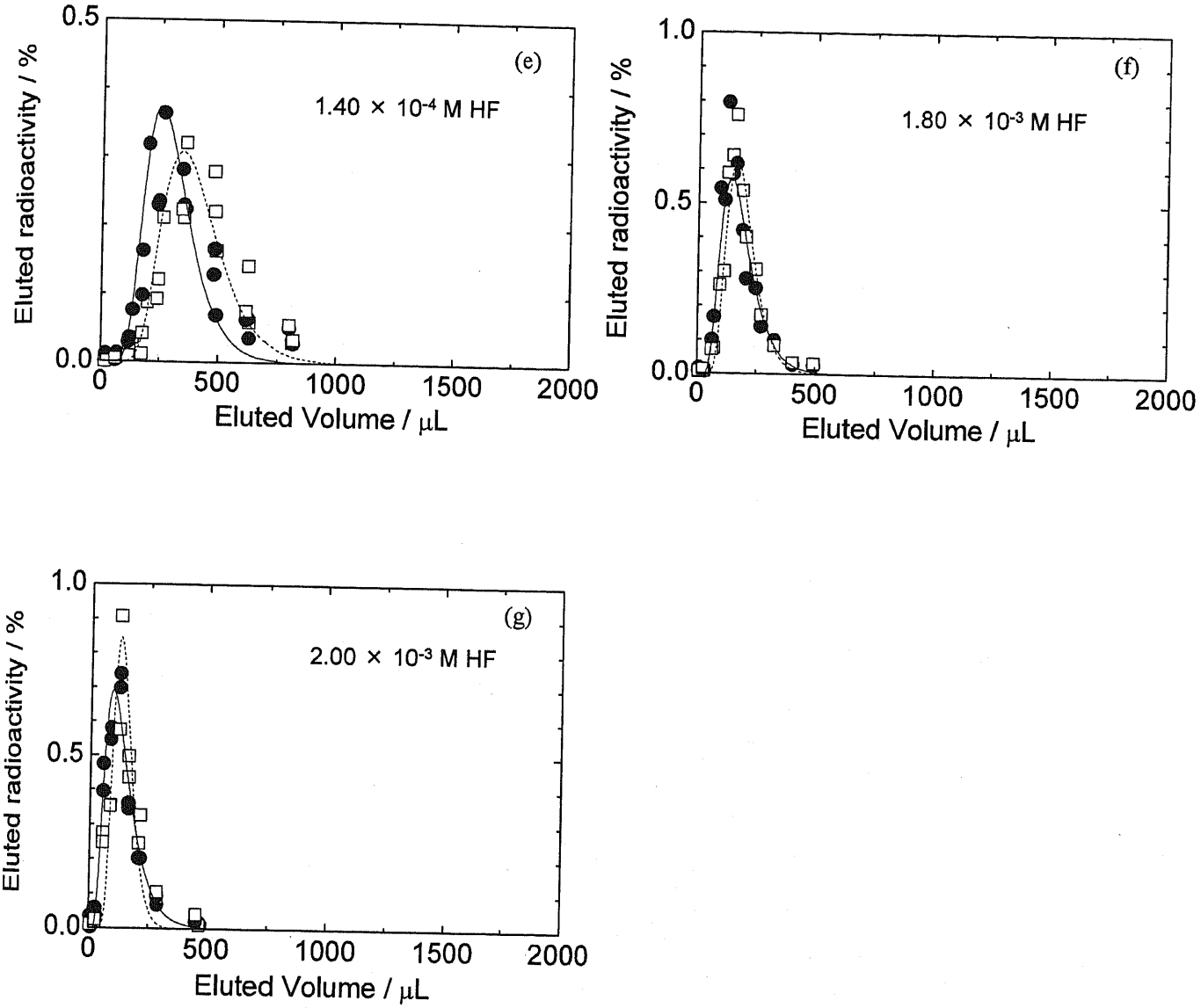

Fig. 3-2. Elution curves of ^{85}Zr and ^{169}Hf in HF/0.10 M HNO_3 solutions with the 1.6 mm i. d. × 7.0 mm columns, ●: Zr and □: Hf. The concentrations of HF are indicated in each figures. The solid and dashed lines indicate the results of the fits by the Glueckauf equation [21].

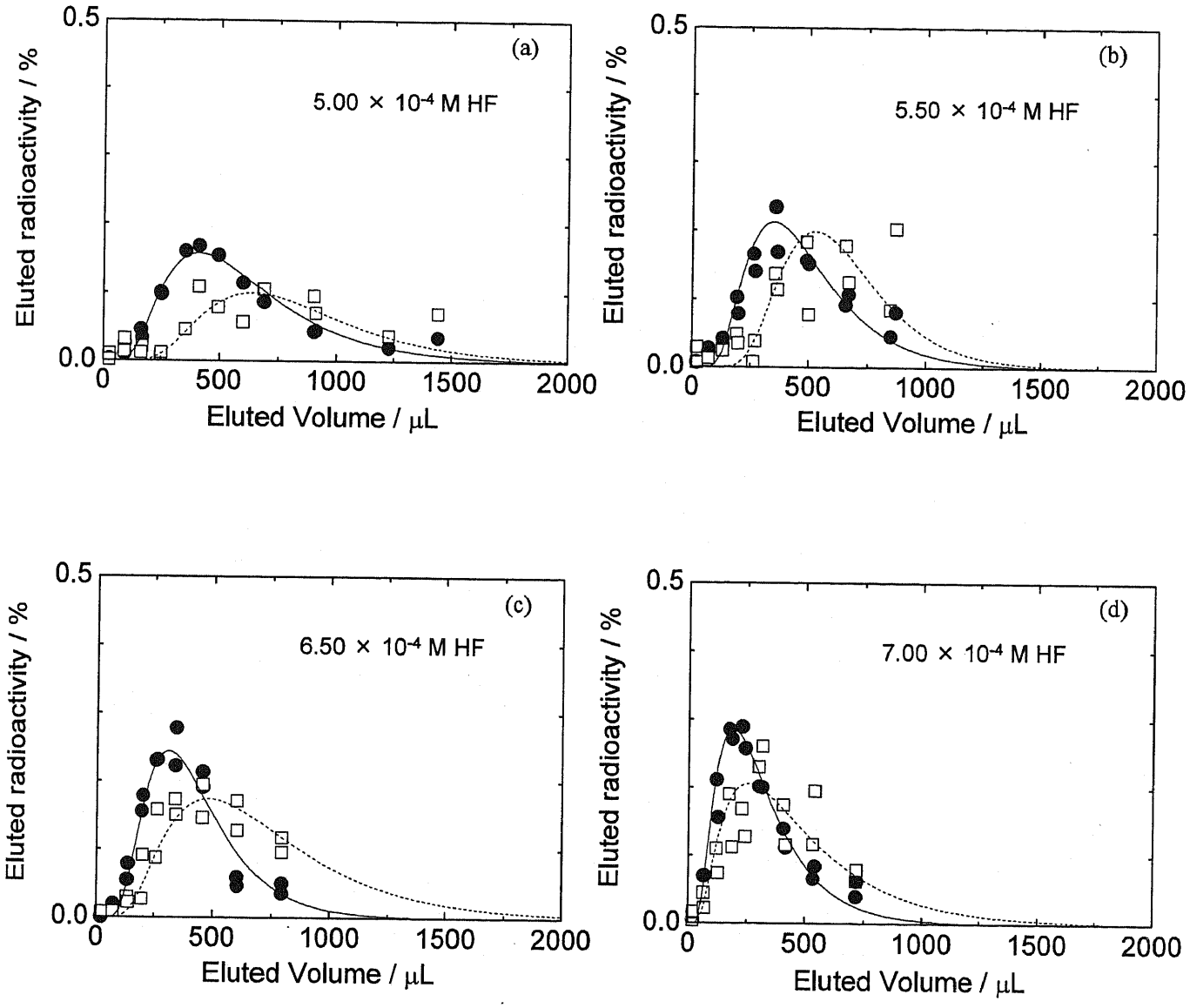

Fig. 3-3. Elution curves of ^{85}Zr and ^{169}Hf in HF/0.10 M HNO_3 solutions with the 1.0 mm i. d. × 3.5 mm columns, ●: Zr and □: Hf. The concentrations of HF are indicated in each figures. The solid and dashed lines indicate the results of the fits by the Glueckauf equation [21].

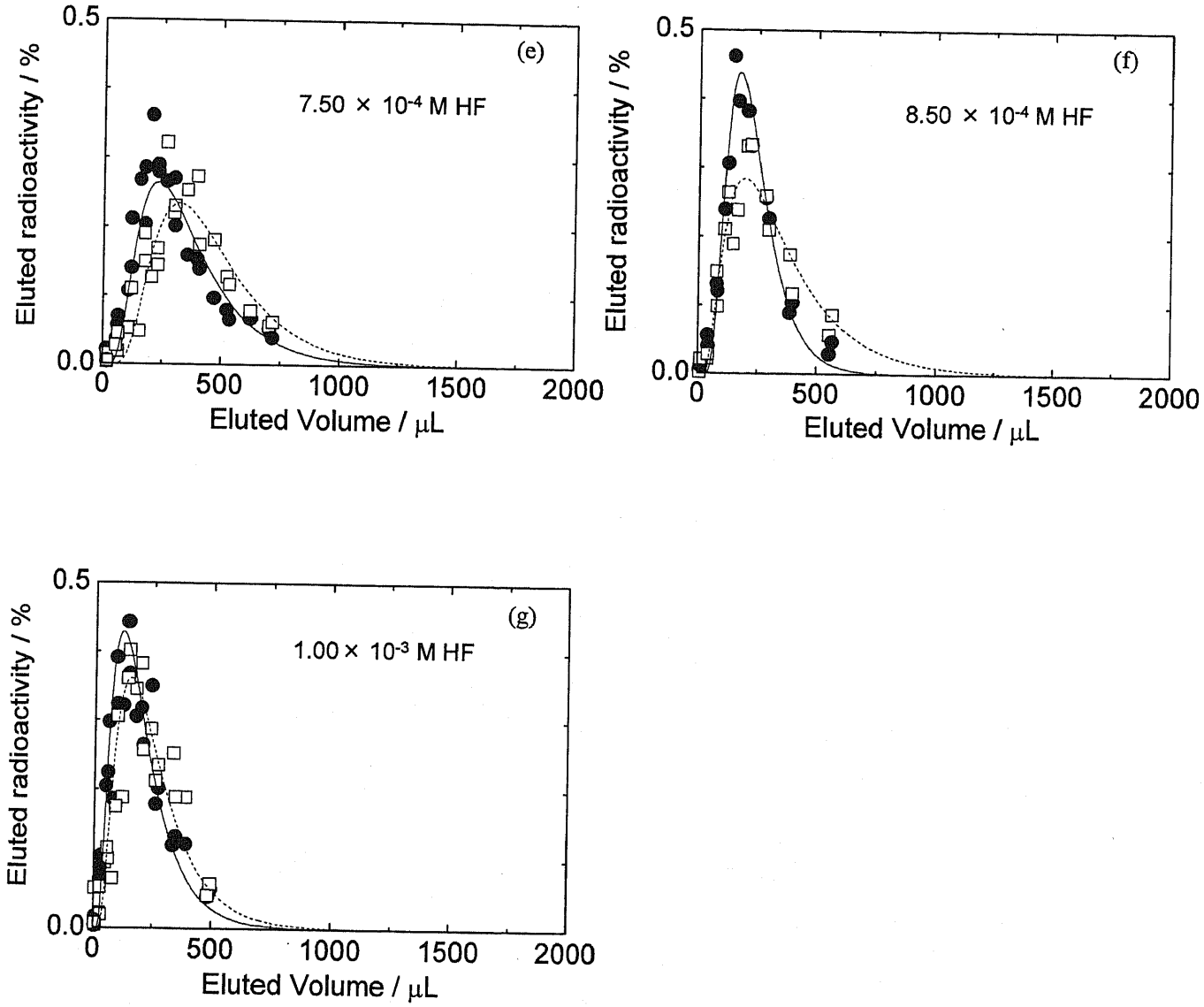

Fig. 3-3. Elution curves of ^{85}Zr and ^{169}Hf in HF/0.10 M HNO_3 solutions with the 1.0 mm i. d. × 3.5 mm columns, ● : Zr and □ : Hf. The concentrations of HF are indicated in each figures. The solid and dashed lines indicate the results of the fits by the Glueckauf equation [21].

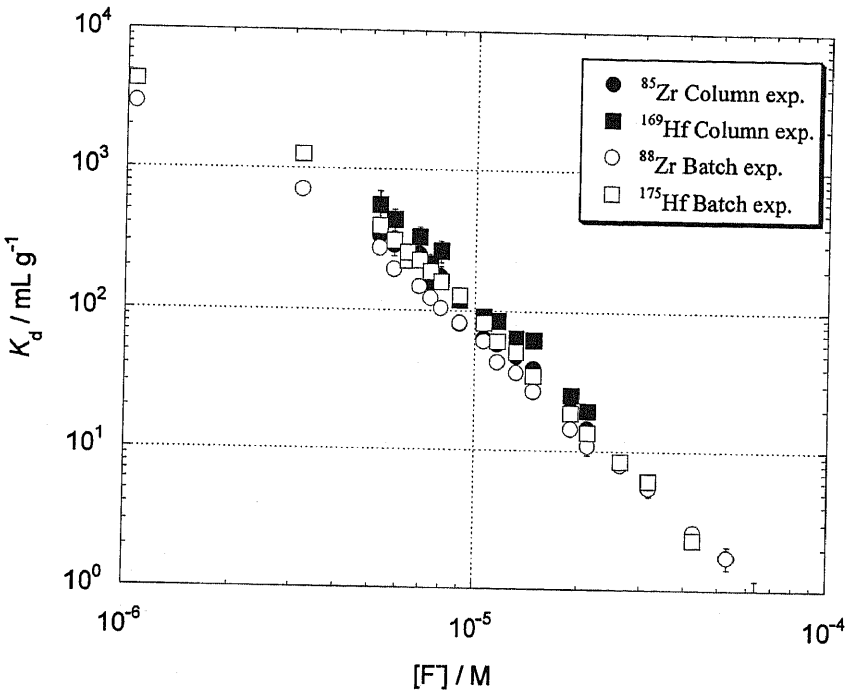

Fig. 3-4. Comparison of distribution coefficients (K_d) of ^{88}Zr and ^{175}Hf in the batch experiment and those of ^{85}Zr and ^{175}Hf in the on-line column chromatographic method in HF/0.10 M HNO_3.

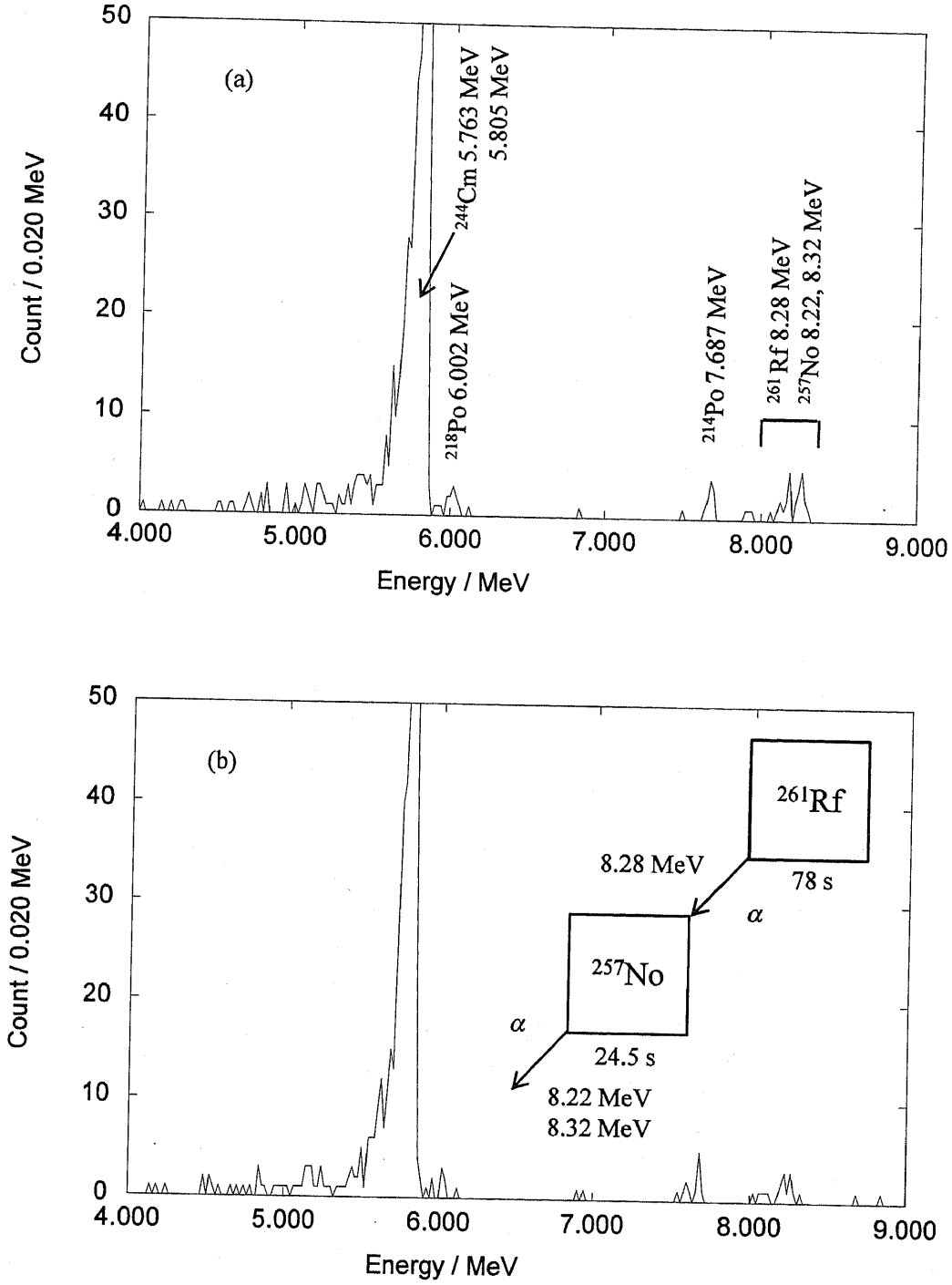

Fig. 3-5. The typical α-particle spectra of samples prepared from the two effluents, fractions 1 (a) and 2 (b), in 2.50×10^{-2} M HF/0.10 M HNO_3.

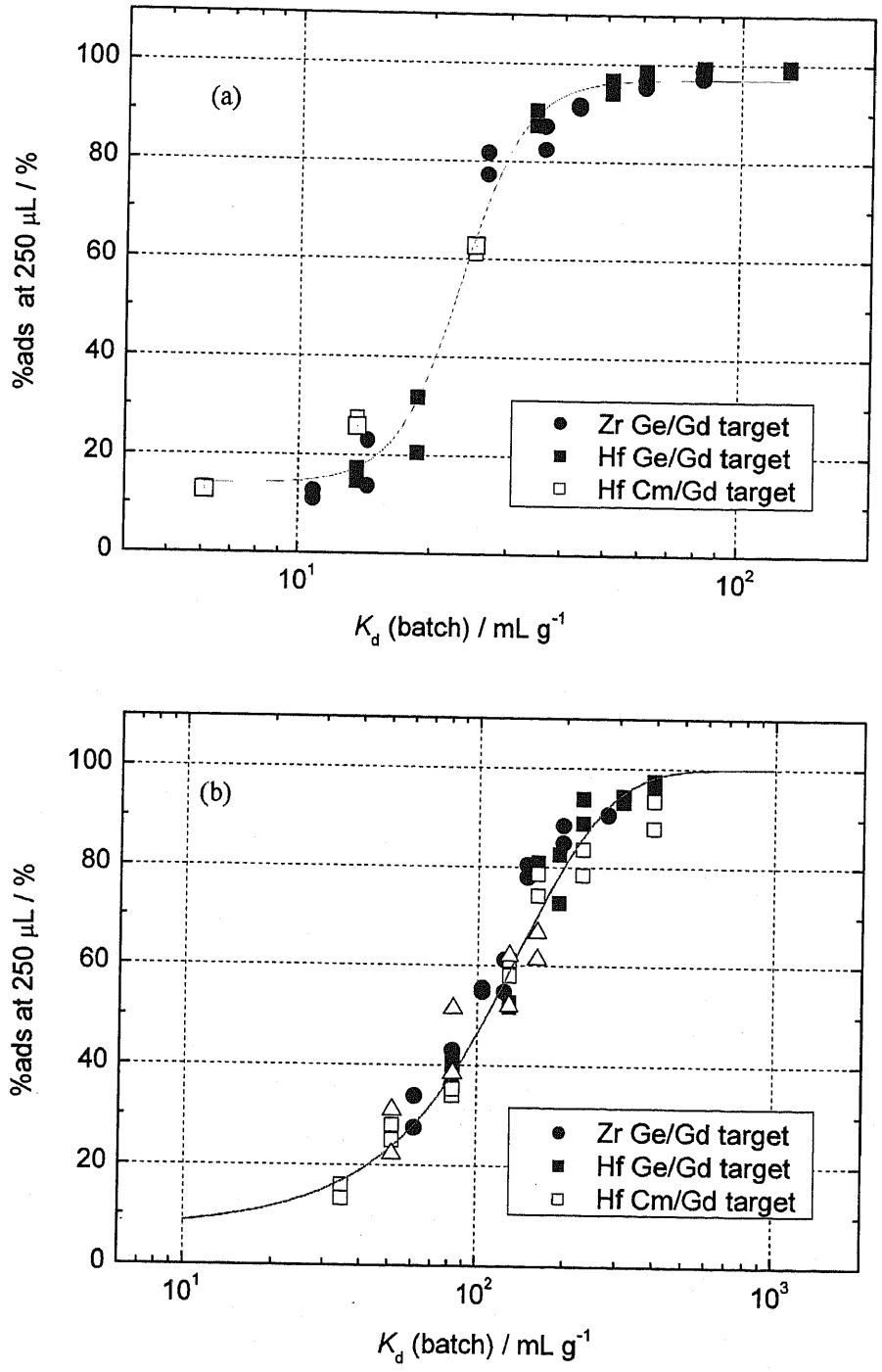

Fig. 3-6. Variations of the percent adsorption values, %ads, of Zr and Hf on the cation-exchange resin CK08Y obtained with the microcolumns, (a) 1.6 mm i.d. × 7.0 mm and (b) 1.0 mm i.d. × 3.5 mm as a function of the distribution coefficient K_d by the batch method.

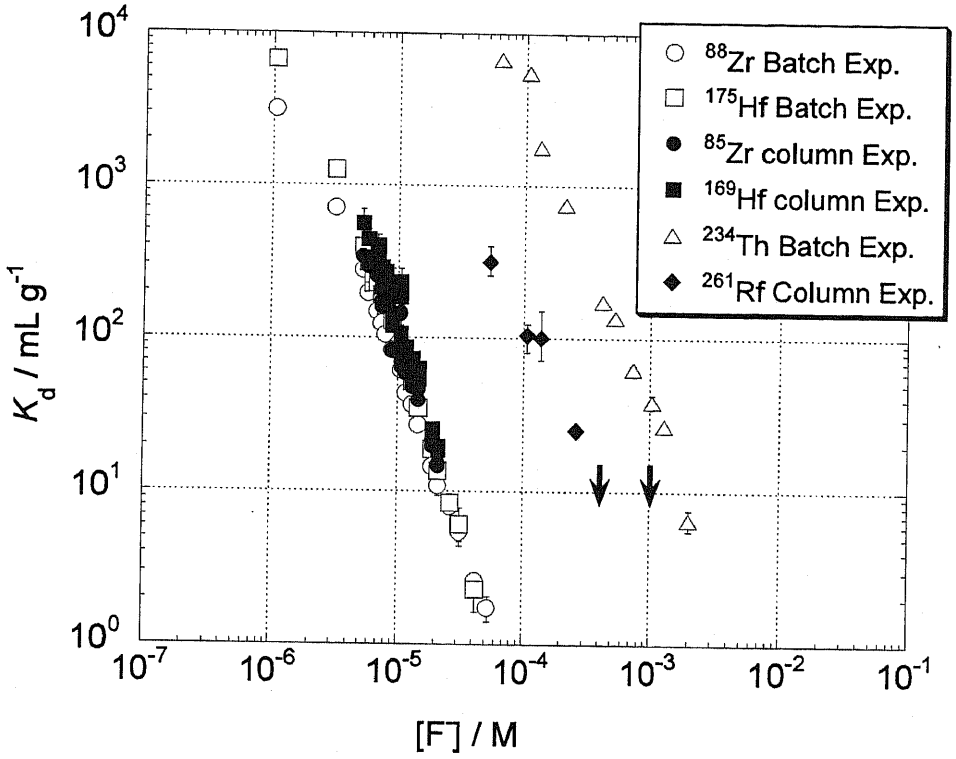

Fig. 3-7. Distribution coefficients (K_d) of Zr, Hf, Th and Rf on the cation-exchange resin (CK08Y) in 0.10 M HNO_3 depending on the concentration of the fluoride ion [F^-].

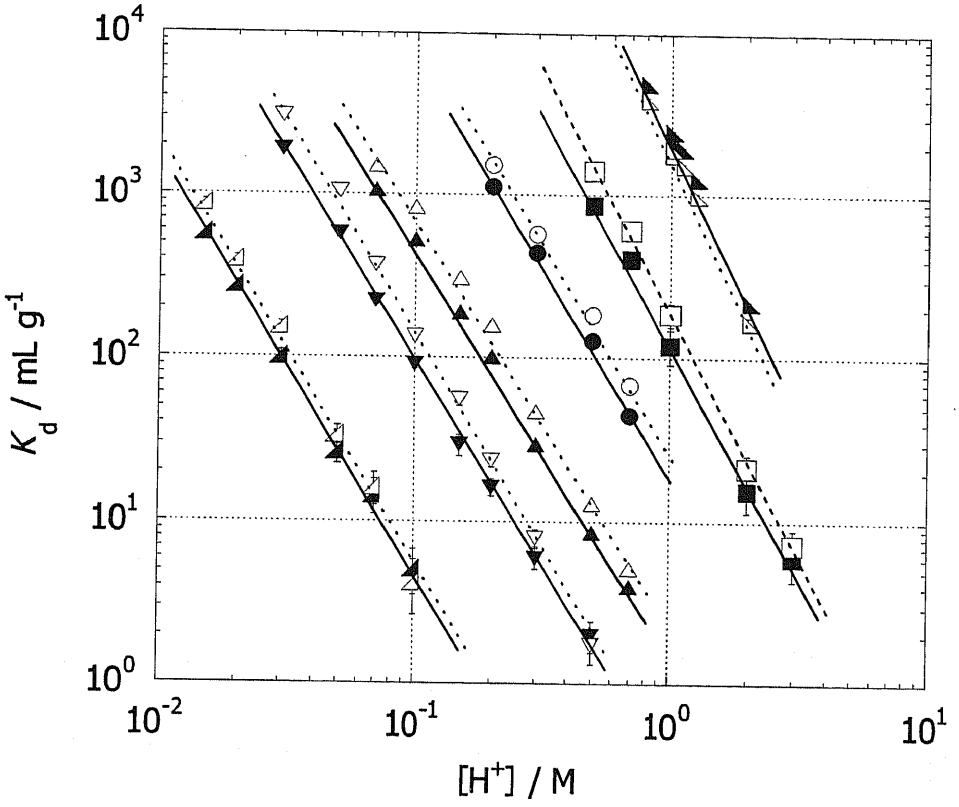

Fig. 3-8. Variation of the K_d values of ^{88}Zr and ^{175} Hf as a function of [H$^+$] at various fluoride ion concentrations [F$^-$] in HF/HNO_3 solutions,

◣ : Zr [F$^-$] = 0 M, ◺ : Hf [F$^-$] = 0 M,

▲ : Zr [F$^-$] = 1.06 × 10^{-7} M, △ : Hf [F$^-$] = 1.06 × 10^{-7} M,

● : Zr [F$^-$] = 5.29 × 10^{-7} M, ○ : Hf [F$^-$] = 5.29 × 10^{-7} M,

▼ : Zr [F$^-$] = 3.17 × 10^{-6} M, ▽ : Hf [F$^-$] = 3.17 × 10^{-6} M,

△ : Zr [F$^-$] = 8.99 × 10^{-6} M, ▲ : Hf [F$^-$] = 8.99 × 10^{-6} M,

◢ : Zr [F$^-$] = 3.17 × 10^{-5} M and ◿ : Hf [F$^-$] = 3.17 × 10^{-5} M.

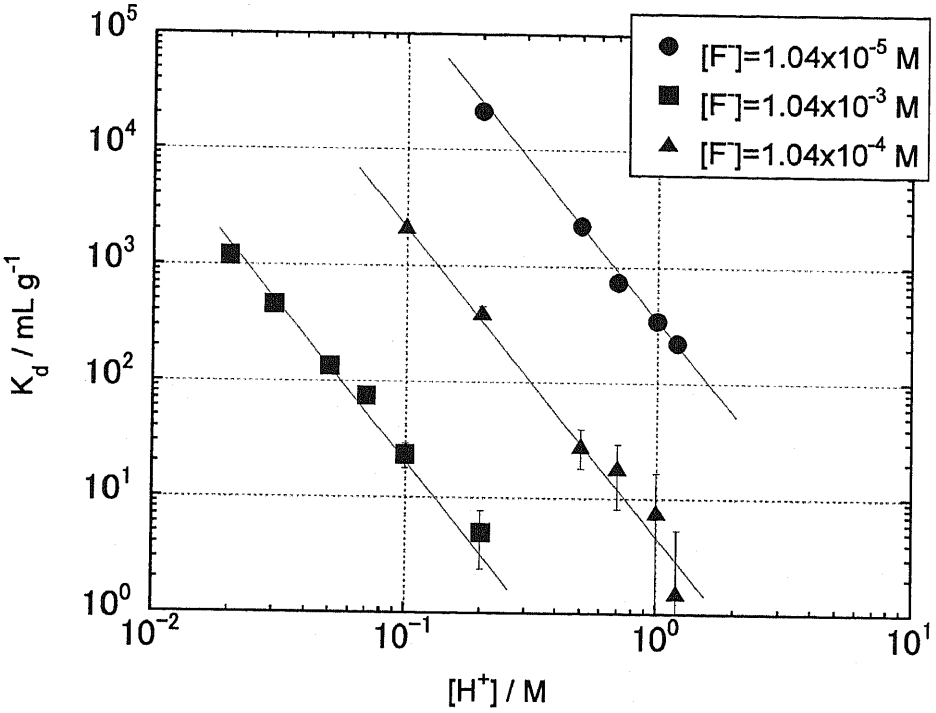

Fig. 3-9. Variation of the K_d values of ^{234}Th as a function of [H$^+$] at various fluoride ion concentrations [F$^-$] in HF/HNO_3 solutions.

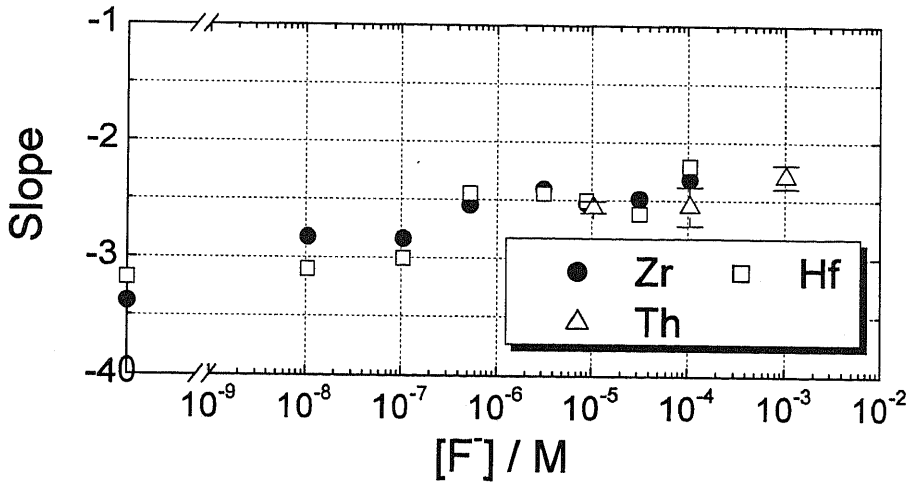

Figure 3-10. Variation of the slopes for ^{88}Zr, ^{175}Hf and ^{234}Th in the $\log K_d$ - $\log[H^+]$ plot as a function of $[F^-]$ in HF/HNO_3.

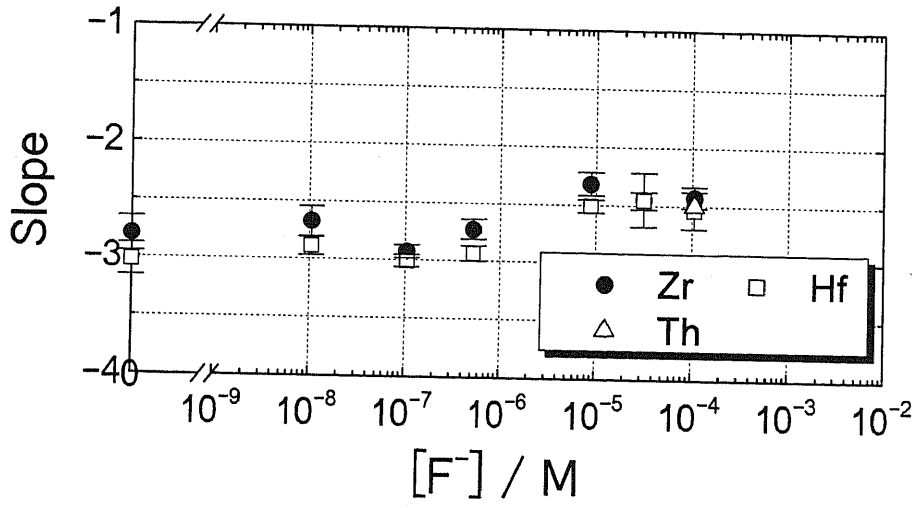

Fig. 3-11. Variation of the slopes for ^{88}Zr, ^{175}Hf and ^{234}Th in the $\log K_d$ - $\log[H^+]$ plot as a function of $[F^-]$ in $HF/HClO_4$.

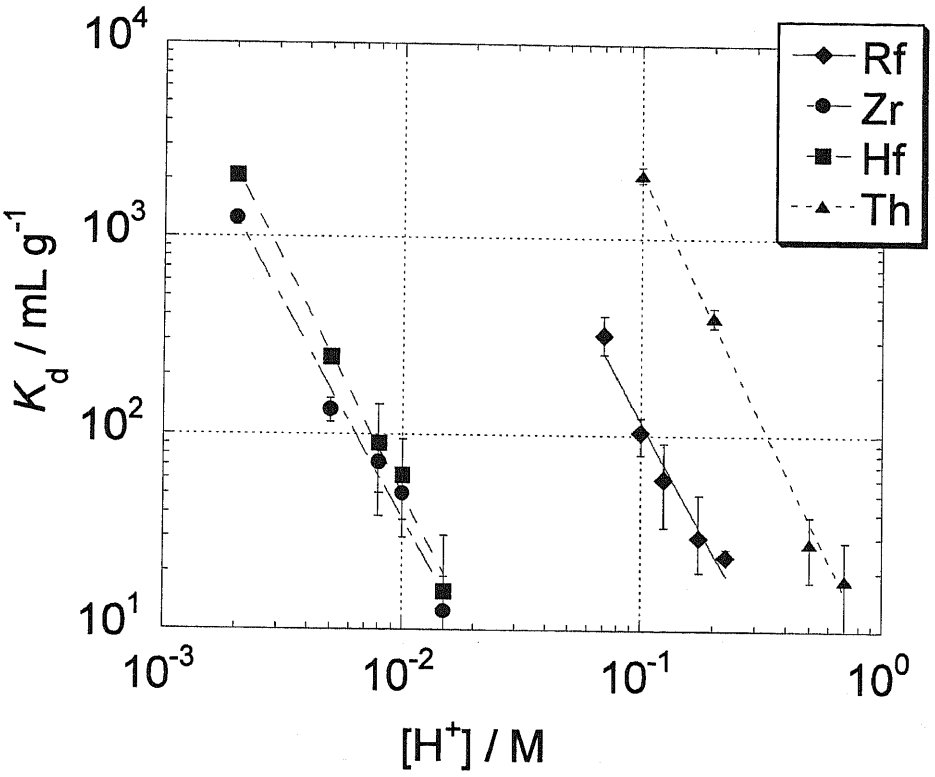

Figure 3-12. Variation of the K_d values of Rf, Zr, Hf and Th at $[F^-] = 1.06 \times 10^{-4}$ M as a function of $[H^+]$.

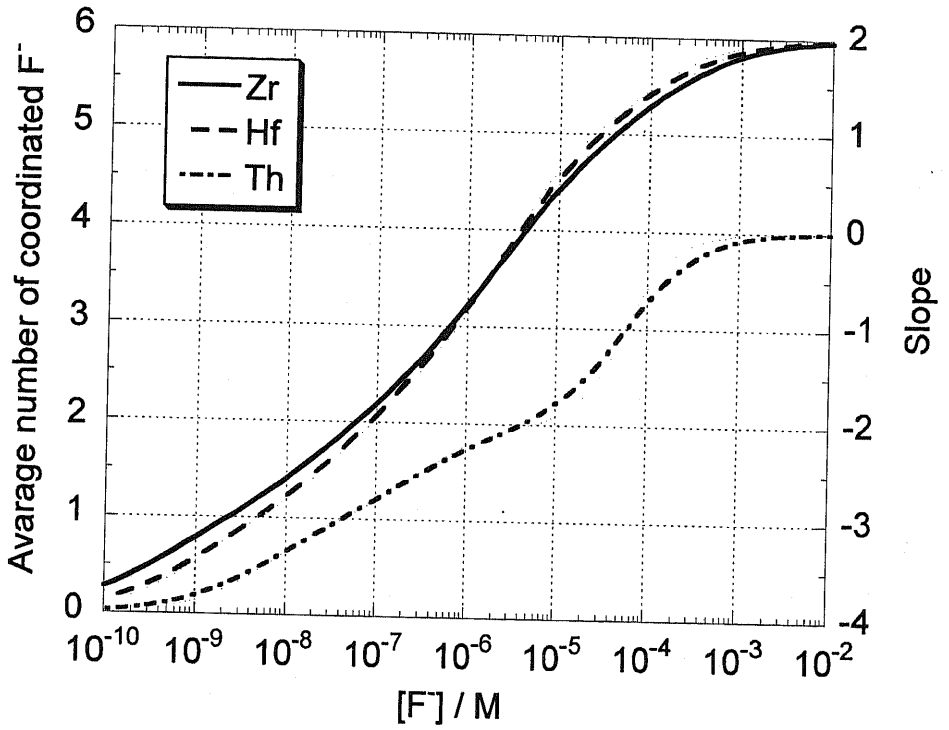

Fig. 3-13. Calculated average number of the coordinated fluoride ion (F^-) to Zr, Hf and Th as a function of [F^-]. Stability constants of fluoro complexes of these ions used are listed in Table 3-4.

Chapter 4

Conclusions

Fluoride complex formation of element 104, rutherfordium (Rf), was studied by cation-exchange chromatography in HF/HNO_3 solutions based on one-atom-at-a-time scale. The μL-order chromatographic apparatus, AIDA, made it possible to perform rapid and repetitive experiments with good statistics, resulting in precise cation-exchange data of Rf.

The nuclide ^{261}Rf ($T_{1/2}$ = 78 s) was synthesized in the $^{248}Cm(^{18}O, 5n)$ reaction with a production rate of about 2 atoms per minute at the JAEA tandem accelerator. Reaction products recoiling from the ^{248}Cm target foil were stopped in He gas loaded with KCl aerosols. The cation-exchange chromatographic behavior of Rf was investigated in the HF/HNO_3 mixed solutions together with the homologues Zr and Hf, and the tetravalent pseudo-homologue Th.

In the HF/0.10 M HNO_3 solution, it was found that the K_d values of Rf decrease with increasing the concentration of the fluoride ion $[F^-]$ as those with the homologues Zr, Hf and Th. This indicates the successive fluoride complex formation of Rf. The order of the adsorption strength on the cation-exchange resin was Zr ~ Hf < Rf < Th.

The K_d values of Rf at $[F^-] = 1.06 \times 10^{-4}$ M were also measured as a function of the hydrogen ion concentration $[H^+]$. The results showed that K_d linearly decrease with increasing $[H^+]$ with the slope of -2.3 ± 0.4 in the $\log K_d$ vs. $\log[H^+]$ plot that corresponds to the average electric charge of the fluoro complexes of Rf on the cation-exchange resin. The average number of the coordinated fluoride ions to Rf on the cation-exchange resin was deduced to be 1.5. In the present condition, RfF^{3+} and/or RfF_2^{2+} are likely to be present on the cation-exchange resin. This tendency was similar to those of Zr, Hf and Th. Thus, it was concluded that Rf, Zr, Hf and Th are present as the same chemical species, MF^{3+} and/or MF_2^{2+} (M = Rf, Zr, Hf or Th) in the

studied solutions.

Due to the predominant electrostatic interaction of the tetravalent group-4 and pseudo group-4 elements with the fluoride ion F^-, a correlation between the ionic radii (IR) and the K_d values was discussed. The experimentally obtained sequence on the fluoride complexation of these elements was agreed with the reverse order of the size of IR. The present result clearly indicated that the size of Rf^{4+} would be in between those of Zr^{4+} and Hf^{4+}, and Th^{4+}.

References

1. M. Schädel (ed.), *The Chemistry of Superheavy Elements*, Kluwer, Dordrecht, **2003.**

2. J. V. Kratz, *Pure Appl. Chem.*, **2003**, *75*, 103.

3. J. V. Kratz, in *Handbook of Nuclear Chemistry*, ed. by A. Vértes, S. Nagy and Z. Klencsár, Kluwer, Dordrecht, **2003**, vol. 2, pp. 323-395.

4. M. Schädel, *Angew. Chem. Int. Ed.*, **2006**, *45*, 368.

5. D. C. Hoffman, D. M. Lee and V. Pershina, in *The Chemistry of the Actinides and Transactinide Elements*, 3rd ed., ed. by L. R. Morss, N. M. Edelstein and J. Fuger, Springer, Dordrecht, **2006**, vol. 3, pp. 1652-1752.

6. V. Pershina, *Chem. Rev.* **1996**, *96*, 1977.

7. V. Pershina, in *The Chemistry of Superheavy Elements*, ed. by M. Schädel, Kluwer, Dordrecht, **2003**, Chap. 2, pp. 31-94.

8. S. Hofmann, in *The Chemistry of Superheavy Elements*, ed. by M. Schädel, Kluwer, Dordrecht, **2003**, Chap. 1, pp. 1-30.

9. R. Guillaumont, A. Tuerler, A. Peneloux and P. Delamoye, *Radiochim. Acta,* **1991**, *46*, 169.

10. R. Guillaumont, J. P. Adloff and A. Peneloux, *Radiochim. Acta,* **1991**, *46*, 169.

11. J. V. Kratz, in *Heavy Elements and Rerated New Phenomena Vol. 1,* ed. by W. Greiner and R. K. Gupta, World Scientific, Singapore,**1999**, pp. 129-193.

12. R. Silva, J. Harris, M. Nurmia, K. Eskola and A. Ghiorso, *Inorg. Nucl. Chem. Lett.*, **1970**, *6*, 871.

13. E. K. Hulet, R. W. Lougheed, J. F. Wild. J. H. Landrum, J. M. Nitschke and A. Ghiorso, *J. Inorg. Nucl. Chem.*, **1980**, *42*, 79.

14. I. Zvara, V. Z. Belov, L. P. Chelnikov, V. P. Domanov, M. Hussonois, Yu. S. Morotkin, V. A. Shegolev and M. R. Shalaevski, *Inorg. Nucl. Chem. Lett.*, **1971**, *7*, 1109.

15. C. D. Kacher, K. E. Gregorich, D. M. Lee, Y. Watanabe, B. Kandkhodayan, B. Wierczinski,

M. R. Lane, E. R. Sywester, D. A. Keeney, M. Hendricks and D. C. Hoffman, *Radiochim. Acta,* **1996**, *75*, 135.

16. Z. Szeglowski, H. Bruchertseifer, V. P. Domanov, B. Gleisberg, L. J. Guseva, M. Hussonois, G. S. Tikhomirova, I. Zvara and Y. T. Oganessian, *Radiochim. Acta*, **1990**, *51*, 71.
17. G. Pfrepper, R. Pfrepper, D. Krauss, A. B. Yakushev, S. N. Timokhin and I. Zvara, *Radiochim. Acta*, **1998**, *80*, 7.
18. E. Strub, J. V. Kratz, A. Kronenberg, A. Nähler, P. Thörle, S. Zauner, W. Brüchle, E. Jäger, M. Schädel, B. Schausten, E. Schimpf, Li. Zongwei, U. Kirbach, D. Schumann, D. Jost, A. Türler, M. Asai, Y. Nagame, M. Sakama, T. Tsukada, H. W. Gäggeler and J. P. Glatz, *Radiochim. Acta*, **2000**, *88*, 265.
19. A. Kronenberg, K. Eberhardt, J. V. Kratz, P. K. Mohapatra, A. Nähler, P. Thörle, W Brüchle, M Schädel and A Türler, *Radiochim. Acta,* **2004**, *88*, 265.
20. D. Schumann, H. Nitsche, St. Taut, D. T. Jost, H. W. Gäggeler, A. B. Yakushev, G. V. Buklanov, V. P. Domanov, D. T. Lien, B. Kubica, R. Misiak and Z. Szeglowski, *J. Alloys Comp.*, **1998**, *271-273*, 307.
21. E. Glueckauf, *Trans. Faraday Soc.*, **1955**, *51*, 34.
22. H. Haba, K. Tsukada, M. Asai, A. Toyoshima, K. Akiyama, I. Nishinaka, M. Hirata, T. Yaita, S. Ichikawa, Y. Nagame, K. Yasuda, Y. Miyamoto, T. Kaneko, S. Goto, S, Ono, T. Hirai, H. Kudo, M. Shigekawa, A. Shinohara, Y. Oura, H. Nakahara, K. Sueki, H. Kikunaga, N. Kinoshita, N. Tsuruga, A. Yokoyama, M. Sakama, S. Enomoto, M. Schädel, W. Brüchle and J. V. Kratz, *J. Am. Chem. Soc.*, **2004**, *126*, 5219.
23. A. Toyoshima, H. Haba, K Tsukada, M. Asai, K. Akiyama, I. Nishinaka, Y. Nagame, D. Saika, K. Matsuo, W. Sato, A. Shinohara, H. Ishizu, M. Ito, J. Saito, S. Goto, H. Kudo, H.

Kikunaga, N. Kinoshita, C. Kato, A. Yokoyama and K. Sueki, *J. Nucl. Radiochem. Sci.*, **2004**, *5*, 45.

24. A. Toyoshima, H. Haba, K. Tsukada, M. Asai, K. Akiyama, S. Goto, W. Sato, Y. Ishii, I. Nishinaka, T. K. Sato, Y. Nagame, Y. Tani, H. Hasegawa, K. Matsuo, D. Saika, Y. Kitamoto, A. Shinohara, M. Ito, J. Saito, H. Kudo, A. Yokoyama, M. Sakama, K. Sueki, Y. Oura, H. Nakahara, M. Schädel, W. Brüchle and J. V. Kratz, *Radiochim. Acta,* **2008**, *96*, 125.
25. A. Tüler and K. E. Gregorich, in *The Chemistry of Superheavy Elements*, ed. by M. Schädel, Kluwer, Dordrecht, **2003**, Chap. 4, pp. 117-157.
26. Y. Nagame, M. Asai, H. Haba, S. Goto, K. Tsukada, I. Nishinaka, K. Nishio, S. Ichikawa, A. Toyoshima, K. Akiyama, H. Nakahara, M. Sakama, M. Schädel, J. V. Kratz, H. Gäggeler and A. Türler, *J. Nucl. Radiochem. Sci.*, **2002**, *3,* 85.
27. E. Stender, N. Trautmann and G. Herrman, *Radiochem. Radioanal. Lett.*, **1980**, *42*, 291.
28. Y. Nagame, H. Haba, K. Tsukada, M. Asai, K. Akiyama, M. Hirata, I. Nishinaka, S. Ichikawa, H. Nakahara, S. Goto, T. Kaneko, H. Kudo, A. Toyoshima, A. Shinohara, M. Schädel, J. V. Kratz, H. W. Gäggler and A. Türler, *Czech. J. Phys. Suppl. A,* **2003**, *53*, 299.
29. M. Schädel, W. Brüchle, E. Jäger, E. Schimpf, J. V. Kratz, U. W. Sherer and H. P. Zimmermann, *Radiochim. Acta,* **1989**, *48*, 171.
30. M. Plaisance, R. Guillaumont, *Radiochim. Acta*, **1969**, *12*, 32.
31. S. Ahrland, D. Karipides and B. Norén, *Acta Chem. Scand.*, **1963**, *17*, 411.
32. B. Norén, *Acta Chem. Scand.*, **1967**, *21*, 2449.
33. E. L. Zebroski, H. W. Alter and F. K. Heumann, *J. Am. Chem. Soc.*, **1951**, *73*, 5646.
34. R. M. Smith and A. E. Martell, NIST Standard Reference Database 46.
35. R. B. Firestone and V. S. Shirley, in *The Table of Isotopes 8th edn*, ed. by J. Wiley and Sons,

Inc., New York, **1996**.

36. M. Asai, K. Tsukada, M. Sakama, S. Ichikawa, T. Ishii, Y. Nagame, I. Nishinaka, K. Akiyama, A. Osa, Y. Oura, K. Sueki, and M. Shibata, *Phys. Rev. Lett.*, **2005**, *95*, 102502.
37. J. Maly, *Science*, **1968**, *160*, 1114.
38. W. Brüchle, *Radiochim. Acta*, **2003**, *91*, 71.
39. R. D. Shannon, *Acta Cryst.*, **1976**, *A32*, 751.
40. R. G. Pearson, *J. Chem. Educ.*, **1968**, *45*, 581-587.
41. R. G. Pearson, *J. Chem. Educ.*, **1968**, *45*, 643-648.

Acknowledgement

I would like to express my deep and sincere gratitude to my supervisor, Professor Hideo Suganuma of Shizuoka University, for all of his support, guidance, and encouragements in the course of this study. I would like to express my thanks to Professor Kenji Okuno, professor Hideaki Kanno Associate Professor Makoto Yanaga and Associate Professor Yasuhisa Oya of Shizuoka University for their valuable suggestions and advice through the study.

I would also especially like to my great appreciation to Dr. Yuichiro Nagame of Japan Atomic Energy Agency (JAEA) for his valuable discussion and suggestions through this study and giving me a chance to the study the chemistry of the superhavy elements. I wish to thank Dr. Kazuki Tsukada, Dr. Masato Asai and Dr. Atsushi Toyoshima of JAEA, and Dr. Hiromitsu Haba of RIKEN for their support, suggestions and discussions. Grateful acknowledgment goes to Mr. Hayato Toume, Dr. Yoshitaka Kasamatsu, Dr. Tetsuya K Sato and Mr. Ichiro Nishinaka (JAEA), Mr. Sunao Miyashita and Dr. Tomotaka Mori (Shizuoka University), Mr. Masami Sakamaki, Associate Professor Shin-ichi Goto and Professor Hisaaki Kudo (Niigata University), Dr. Kazuhiko Akiyama and Associate Professor Yasuji Oura (Tokyo metropolitan University), Mr. Yuki Tashiro and Professor Atsushi Shinohara (Osaka University) and all other collaborators. The present study of Rf was not able to do without their help.

I would like to thank the members of Radiochemistry Research Laboratory, Shizuoka University.

List of Publication

1. **Fluoride Complexation of Element 104, Rutherfordium (Rf), Investigated by Cation-exchange Chromatography**

   Y. Ishii, A. Toyoshima, K. Tsukada, M. Asai, H. Tome, I. Nishinaka, Y. Nagame, S. Miyashita, T. Mori, H. Suganuma, H. Haba, M. Sakamaki, S. Goto, H, Kudo, K. Akiyama, Y. Oura, H. Nakahara, Y. Tashiro, A. Shinohara, M. Schädel, W. brüchle, V. Pershina and J. V. Kratz

   Chemistry Letters, **2008**, *37*, 288-289.

2. **Hexafluoro complex of rutherfordium in mixed HF/HNO_3 solutions**

   A. Toyoshima, H. Haba, K. Tsukada, M. Asai, K. Akiyama, S. Goto, Y. Ishii, I. Nishinaka, T. K. Sato, Yuichi Nagame, Wataru Sato, Yuuki Tani, H. Hasegawa, K. Matsuo, D. Saika, Y. Kitamoto, A. Shinohara, M. Ito, J. Saito, H. Kudo, A. Yokoyama, M. Sakama, K. Sueki, Y. Oura, H. Nakahara, M. Schädel, W. Brüchle and J. V. Kratz

   Radiochimica Acta, **2008**, *96*, 125-134.

3. **Separation of Am^{III} from Eu^{III} using an improved system of flow-counterbalanced capillary electrophoresis**

   T. Mori, Y. Ishii, K. Hayashi, M. Yanaga and H. Suganuma.

   Chemistry Letters, **2008**, *37*, 48–49.

4. **Extraction behavior of rutherfordium into tributylphosphate from hydrochloric acid**

H. Haba, K. Tsukada, M. Asai, A. Toyoshima, Y. Ishii, H. Tome, T. Sato, I. Nishinaka, T. Ichikawa, S. Ichikawa, Y. Nagame, W, Sato, K. matsuo, Y. Kitamoto, Y. Tashiro, A. Shinohara, J. Saito, M. Ito, T. Ikezawa, M. Sakamaki, S. Goto, H. Kudo, H. Kikunaga, M. Arai, S. Kamataki, A. Yokoyama, K. Akiyama, K. Sueki, Y. Oura, M. Schädel, W. Brüchle and J. V. Kratz

Radiochimica Acta, **2007**, *95*, 1–6.

5. **Chemical studies on rutherfordium (Rf) at JAERI**

Y. Nagame, K. Tsukada, M. Asai, A. Toyoshima, K. Akiyama, Y. Ishii, T. Kaneko-Sato, M. Hirata, I. Nishinaka, S. Ichikawa, H. Haba, S. Matsuo, D. Saika, Y. Kitamoto, H. Hasegawa, Y. Tani, W. Sato, A. Shinohara, M. Ito, J. Saito, S. Goto, H. Kudo, H. Kikunaga, N. Kinoshita, A. Yokoyama, K. Sueki, Y. Oura, H. Nakahara, M. Sakama, M. Schädel, W. Brüchle and J. V. Kratz

Radiochimica Acta, **2005**, *93*, 519–526.

6. **Cm^{3+}-F^- interaction in a mixed system of methanol and water**

I. Satoh, T. Watanabe, Y. Ishii, M. Kawasaki and H. Suganuma

Journal of Radioanalytical and Nuclear Chemistry, **2003**, *255*, 249–251.

7. **Atom-at-a-time chemistry of the transactinide element, rutherfordium (element 104) –Towards experimental verification of relativistic effects in chemical properties-**

Y. Nagame, K. Tsukada, M. Asai, A. Toyoshima, K. Akiyama, Y. Ishii, I. Nishinaka, T. K. Sato, M. Hirata, T. Ichikawa, H. Haba, S. Goto and M. Sakama

Proceedings of the 5th Italy-Japan Symposium, Recent Achievements and Perspectives in Nuclear Physics, Naples, Italy, 3-7 November, 2004, World Scientific, 2005, pp. 295 – 306.

8. **Chemical studies of the transactinide elements at JAEA**

Y. Nagame, K. Akiyama, M. Asai, S. Goto, H. Haba, M. Hirata, Y. Ishii, I. Nishinaka, H. Tome, A. Toyoshima and K. Tsukada

Proceedings of the 6th China-Japan Joint Nuclear Physics Symposium –Nuclear Physics Trends-, May 16-20, 2006, Shanghai, China, (AIP Conference Proceedings 865, AIP, 2006), pp. 165-172.

9. **Aqueous chemistry of the transactinide element, rutherfordium (Rf)**

Y. Nagame, M. Asai, H. Haba, H. Hirata, Y. Ishii, I. Nishinaka, A. Toyoshima and K. Tsukada

Lecture Series on Computer and Computational Sciences, **2006**, *7*, 927-930.